

1 **All about Nitrite: Exploring Nitrite Sources and Sinks in the Eastern Tropical North**

2 **Pacific Oxygen Minimum Zone**

3

4 John C. Tracey^{1,2}, Andrew R. Babbin³, Elizabeth Wallace¹, Xin Sun^{1,4}, Katherine L. DuRussel^{1,}

5 ⁵, Claudia Frey^{1,6}, Donald E. Martocello III³, Tyler Tamasi³, Sergey Oleynik¹, and Bess B.

6 Ward¹

7

8 ¹ Department of Geosciences, Princeton University, Guyot Hall, Princeton, NJ, USA 08544

9 ² Department of Biology and Paleo Environment, Lamont Doherty Earth Observatory, Columbia
10 University, Palisades, NY, USA 10964

11 ³ Department of Earth, Atmospheric and Planetary Sciences, Massachusetts Institute of
12 Technology, Cambridge, MA, USA 02138

13 ⁴ Department of Global Ecology, Carnegie Institution for Science, Stanford, CA, USA 94305

14 ⁵ Department of Civil and Environmental Engineering, Northwestern University, Evanston, IL,
15 USA 60208

16 ⁶ Department of Environmental Sciences, University of Basel, Bernoullistrasse 30, 4056 Basel,
17 Switzerland

18

19 *Correspondence to:* John C. Tracey (jt16@princeton.edu)

20

21

22

23

24

25

26

27

28

29 **Abstract**

30 Oxygen minimum zones (OMZs), due to their large volumes of perennially deoxygenated
31 waters, are critical regions for understanding how the interplay between anaerobic and aerobic
32 nitrogen (N) cycling microbial pathways affects the marine N budget. Here we present a suite of
33 measurements of the most significant OMZ N cycling rates, which all involve nitrite (NO_2^-) as a
34 product, reactant, or intermediate, in the Eastern Tropical North Pacific (ETNP) OMZ. These
35 measurements and comparisons to data from previously published OMZ cruises present
36 additional evidence that NO_3^- reduction is the predominant OMZ N flux, followed by NO_2^-
37 oxidation back to NO_3^- . The combined rates of both of these N recycling processes were
38 observed to be much greater (up to nearly 200x) than the combined rates of the N loss processes
39 of anammox and denitrification, especially in waters near the anoxic / oxic interface. We also
40 show that NO_2^- oxidation can occur when O_2 is maintained near 1 nM by a continuous purge
41 system, NO_2^- oxidation and O_2 measurements that further strengthen the case for truly anaerobic
42 NO_2^- oxidation. We also evaluate the possibility that NO_2^- dismutation provides the oxidative
43 power for anaerobic NO_2^- oxidation. The partitioning of N loss between anammox and
44 denitrification differed widely from stoichiometric predictions of at most 29% anammox; in fact,
45 N loss rates at many depths were entirely due to anammox. Our new NO_3^- reduction, NO_2^-
46 oxidation, dismutation, and N loss data shed light on many open questions in OMZ N cycling
47 research, especially the possibility of truly anaerobic NO_2^- oxidation.

48

49 **1. Introduction**

50 Nitrogen (N) is essential for life because of its prominent role in DNA, RNA, and protein
51 chemistry. As a result, N limits biological productivity in many marine environments. The

52 dissimilatory biological N loss and recycling pathways are traditionally understood to be strictly
53 separated by O₂ tolerance. The N loss processes of denitrification, the stepwise reduction of
54 NO₃⁻ to N₂, and anaerobic ammonium oxidation (anammox), the oxidation of NH₄⁺ with NO₂⁻ to
55 make N₂, require low O₂ while the N recycling pathways of NH₄⁺ oxidation to NO₂⁻ and NO₂⁻
56 oxidation to NO₃⁻ are viewed as obligately aerobic. Importantly, NO₂⁻ is a product, reactant, or
57 intermediate in all these pathways. Therefore, developing an understanding of NO₂⁻ sources and
58 sinks is essential for a complete understanding of marine N biogeochemistry.

59 Oxygen minimum zones (OMZs) and sediments are the two main marine environments
60 where N loss occurs. There are three major OMZs, the Eastern Tropical North Pacific (ETNP),
61 the Eastern Tropical South Pacific (ETSP), and the Arabian Sea, which occupy 0.1 - 1% of total
62 ocean volume, depending on the O₂ threshold used (Codispoti and Richards, 1976; Naqvi, 1987;
63 Bange et al., 2000; Codispoti et al., 2005; Lam and Kuypers, 2011). Importantly, the OMZ water
64 column is not completely deoxygenated from top to bottom; OMZs are characterized by an
65 oxygenated surface, a depth interval of steeply declining O₂ around the mixed layer depth, called
66 the oxycline, an oxygen deficient zone (ODZ) spanning several hundred meters where O₂
67 declines below the detection limit of common shipboard CTD O₂ sensors, and then a second,
68 gradual, oxycline that transitions to oxygenated deep water. Despite OMZ regions' small size,
69 they are responsible for 30-50 % of total marine N loss (DeVries et al., 2013), a magnitude
70 significant for the global marine N budget. In this work, in order to answer several open
71 questions about OMZs and marine N cycling, we conducted a suite of ¹⁵N stable isotope
72 measurements of the most important N cycling microbial pathways in OMZs. We report the N
73 loss rates of anammox and denitrification, as well as the N recycling rates of NO₃⁻ reduction,
74 NO₂⁻ oxidation, and NH₄⁺ oxidation, all of which involve NO₂⁻.

75 A distinctive feature of OMZs is a secondary nitrite maximum (SNM) (Codispoti et al.,
76 2001; Brandhorst, 1959; Codispoti and Packard, 1980). The highest nitrite concentrations within
77 the SNM can reach 10 μM , much higher than the peak values found in the primary nitrite
78 maximum at the base of the photic zone, which average ~ 100 nM globally (Lomas and
79 Lipschultz, 2006). Several recent works have shown or argued that the SNM's NO_2^- is supplied
80 via high rates of the first step of denitrification, NO_3^- reduction to NO_2^- (Lam et al., 2009; Lam
81 and Kuypers, 2011; Kalvelage et al., 2013; Babbin et al., 2017, 2020). NO_3^- reduction has been
82 proposed (Anderson et al., 1982) to be one-half of a rapid loop where NO_3^- and NO_2^- are
83 recycled through simultaneously occurring NO_3^- reduction and NO_2^- oxidation. This loop has
84 been supported through experimental measurements of both rates (Babbin et al., 2017, 2020;
85 Kalvelage et al., 2013; Lipschultz et al., 1990). In this view, elevated NO_3^- reduction also
86 generates NH_4^+ , via organic matter (OM) remineralization, which enhances anammox at the
87 expense of denitrification in oxycline and upper ODZ waters (Babbin et al., 2020). In this study,
88 we conducted tests to further document this rapid loop's existence and role in enhancing
89 anammox.

90 Recent measurements of NO_2^- oxidation have returned significant rates from both the
91 oxycline and the ODZ, findings that challenge the paradigm that NO_2^- oxidation is an obligately
92 aerobic process. Evidence for high, widespread NO_2^- oxidation rates in low O_2 waters has
93 accumulated from direct rate measurements via ^{15}N tracers (Füssel et al., 2011; Lipschultz et al.,
94 1990; Peng et al., 2015, 2016; Ward et al., 1989; Kalvelage et al., 2013; Tsementzi et al., 2016;
95 Sun et al., 2017, 2021a; Babbin et al., 2017, 2020), models (Buchwald et al., 2015), and ^{15}N
96 natural abundance measurements (Casciotti et al., 2013). Many explanations have been
97 proposed including microaerophilic nitrite oxidizing bacteria (NOB) adapted to low but non-zero

98 O₂ conditions (Penn et al., 2016; Bristow et al., 2016; Tsementzi et al., 2016; Bristow et al.,
99 2017) where the O₂ for these NOB is transiently supplied to previously deoxygenated waters by
100 (1) vertical or horizontal mixing of the ocean surface or nearby oxic water (Casciotti et al., 2013;
101 Tiano et al., 2014; Bristow et al., 2016; Ulloa et al., 2012), even into the anoxic ODZ
102 (Margolskee et al., 2019), or (2) a cryptic O₂ cycle where low-light adapted phototrophs produce
103 O₂ that is consumed by NOB (Garcia-Robledo et al., 2017; Fuchsman et al., 2019).

104 Despite the power of these explanations, they do not preclude the possibility of
105 widespread NOB capable of truly anaerobic NO₂⁻ oxidation, especially in waters from the deep,
106 dark, and deoxygenated ODZ core. This possibility is bolstered by sequencing data that show
107 the presence of an NOB metagenome assembled genome (MAG) with a preference for the
108 deoxygenated ODZ core in the ETSP (Sun et al., 2019) and ODZ core kinetics experiments
109 where O₂ concentrations above 5 μM inhibit NO₂⁻ oxidation (Sun et al., 2021a). Here we build
110 on past stable isotope experimental results by performing additional depth profile experiments
111 with purged waters from the ODZ *and* O₂ manipulation ¹⁵N tracer experiments across a gradient
112 of O₂ concentrations from 1 nM to 10 μM. Our O₂ manipulation experiments, unlike previous
113 studies, were conducted in vessels that were continuously purged throughout each incubation
114 with a precisely calibrated mixture of N₂, O₂, and CO₂. This experimental design allowed us to
115 continuously maintain low O₂ conditions. In addition, our oxygen concentrations in these assays
116 were verified via a LUMOS sensor, a sensor class with a detection limit of 0.5 nM O₂ (Lehner et
117 al., 2015). Together, these method improvements convincingly show that the O₂ contamination
118 observed to occur in Niskin sampling (Garcia-Robledo et al., 2016, 2021) is removed and that
119 vanishingly low O₂ is maintained throughout the experiment.

120 Anaerobic NO_2^- oxidation would require an alternative oxidant other than O_2 . Many
121 candidates have been proposed (Sun et al., 2023) for this oxidant including IO_3^- (Babbin et al.,
122 2017), Mn^{4+} , Fe^{3+} (Sun et al., 2021a), the anammox core metabolism (Sun et al., 2021a), the
123 observed reversibility of the nitrite oxidoreductase enzyme (Wunderlich et al., 2013; Kemeny et
124 al., 2016; Koch et al., 2015; Buchwald and Wankel, 2022), and NO_2^- dismutation (Babbin et al.,
125 2020; Füssel et al., 2011; Sun et al., 2021a). Due to multiple considerations such as very low
126 IO_3^- in the ODZ core (Moriyasu et al., 2020), low favorability of Mn^{4+} or Fe^{3+} mediated NO_2^-
127 oxidation at marine pH values (Luther, 2010), low anammox rates that do not explain the
128 observed stoichiometry of NO_2^- oxidation to anammox (Kalvelage et al., 2013; Babbin et al.,
129 2020; Sun et al., 2021a), and the inability of the enzyme hypothesis to account for structural and
130 phylogenetic differences in the NXR of the four NOB genera (Buchwald and Wankel, 2022;
131 Sun et al., 2019), we conducted experiments to test the remaining most plausible hypothesis:
132 NO_2^- dismutation.

133 NO_2^- dismutation (Eq. (R4)) is energetically favorable (Strohm et al., 2007; Van de
134 Leemput et al., 2011) although it has not been detected in nature. The reaction is proposed to
135 occur in three steps (Eq. (R1-3)) (Babbin et al., 2020) and DNA sequences that encode possible
136 enzymes for steps two and three (Eqs. (R2, R3)) have been found in ODZ core metagenomic
137 reads and MAGs (Padilla et al., 2016; Babbin et al., 2020). While these sequences were not
138 classified as NOB, they do indicate that parts of the pathway could occur in OMZs. If
139 discovered in OMZs, NO_2^- dismutation would be another N loss pathway, albeit one
140 indistinguishable from denitrification since the ^{15}N atoms in $^{30}\text{N}_2$ come from $^{15}\text{NO}_2^-$ in both
141 pathways. Here we evaluate the hypothesis that NO_2^- dismutation is a significant mechanism for
142 NO_2^- oxidation under low O_2 , by searching for product inhibition, the inhibition of both NO_2^-

143 oxidation and $^{30}\text{N}_2$ production (i.e. denitrification) in response to addition of NO_3^- , substrate
144 stimulation (increases in both $^{30}\text{N}_2$ production and NO_2^- oxidation in response to addition of
145 $^{15}\text{NO}_2^-$), and by comparing the NO_2^- oxidation to the produced $^{30}\text{N}_2$ ratio. A ratio near the 3:1
146 stoichiometry of dismutation ($3 \text{NO}_3^- : 1 \text{N}_2$, Eq. (R4)) would indicate that dismutation could
147 explain the NO_2^- oxidation measured in the ODZ core.



152 A final area of OMZ biogeochemistry that we investigate is the relative balance between
153 anammox and denitrification and these pathways' relationships to the rapid NO_2^- oxidation /
154 NO_3^- reduction loop. After the discovery of anammox, many OMZ studies (Kavelage et al.,
155 2013; Kuypers et al., 2005; Hamersley et al., 2007; Jensen et al., 2011; Thamdrup et al., 2006;
156 Lam et al., 2009), but not all (Ward et al., 2009; Bulow et al., 2010; Dalsgaard et al., 2012) have
157 reported that anammox is the dominant N loss flux in OMZs, a surprising difference from the
158 stoichiometric based prediction that OMZ N loss should be at most 29% anammox (Dalsgaard et
159 al., 2003). While the first wave of these studies did not realize that vial septa were introducing
160 O_2 into the incubations, many studies after this discovery observed the same result (Kavelage et
161 al., 2013; Jensen et al., 2011; Babbin et al., 2020). The prediction of a 29% anammox partition
162 assumes that all NH_4^+ for anammox was derived from remineralization of OM with a mean
163 marine C:N ratio through complete denitrification of NO_3^- to N_2 (Dalsgaard et al., 2003, 2012).
164 Anammox rates exceeding 29% of total N loss would therefore require an additional source of
165 NH_4^+ beyond current observations of denitrification and the resulting NH_4^+ remineralization.

166 The best supported explanations for elevated anammox are that (1) denitrification is the
167 NH_4^+ source, but that complete denitrification peaks episodically in response to OM quality
168 while anammox occurs at a slow, consistent, low rate (Ward et al., 2008; Thamdrup et al., 2006;
169 Babbin et al., 2014; Dalsgaard et al., 2012). The snapshots afforded by isotopic incubations on
170 cruises could therefore easily miss episodes of high complete denitrification. (2) Denitrifiers
171 have a strong preference for particles (Ganesh et al., 2013, 2015; Fuchsman et al., 2017) and
172 CTD samples do not capture marine particles very well (Suter et al., 2017). As a result,
173 differences from the expected percent N loss partition in water column samples are due to
174 missing denitrifiers. (3) The rapid loop between NO_3^- and NO_2^- described previously functions
175 as an “engine” to generate NH_4^+ for anammox at the expense of denitrification. The observed
176 magnitudes of NO_3^- reduction and NO_2^- oxidation and these processes’ ability to produce NH_4^+
177 from the remineralization of OM with standard C:N ratios without complete denitrification make
178 this an additional logical hypothesis.

179 The third hypothesis, the $\text{NO}_2^-/\text{NO}_3^-$ loop, is supported by several pieces of evidence.
180 Firstly, ‘omics studies have revealed widespread modular denitrification in OMZs (Sun et al.,
181 2021b; Fuchsman et al., 2017). Furthermore, experimental studies have shown that as NO_3^-
182 reduction increases near the coast, anammox rates also increase (Kalvelage et al., 2013). Our
183 study’s considerable number of data points, as well as our ability to compare results to rate
184 measurements obtained from identical methods on previous cruises offers a unique chance to test
185 both the variable denitrification and rapid loop hypotheses for elevated anammox rates.

186 OMZs are essential regions for the marine N cycle; however, the biogeochemistry of
187 OMZs may currently be in flux due to anthropogenic pressures. Observational studies have
188 reported decreases in O_2 across the Pacific (Ito et al., 2017) and the expansion of denitrification

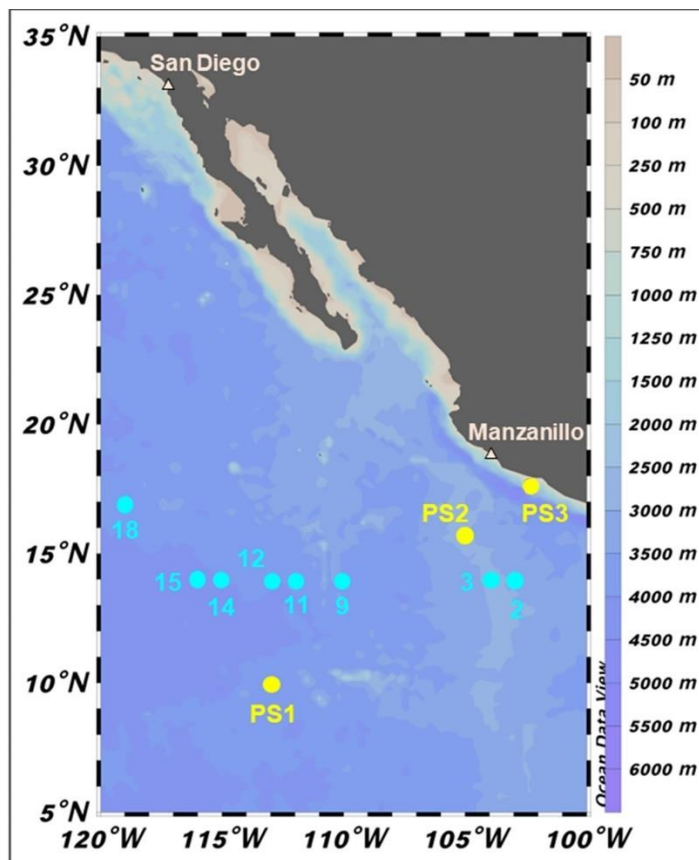
189 and anoxia in the ETNP (Horak et al., 2016). Modeling studies suggest that OMZ volume will
190 continue to grow in the near future, with uncertain impacts (Stramma et al., 2008; Keeling et al.,
191 2010; Busecke et al., 2022). As a result, it is important to develop a thorough understanding of
192 OMZ N cycling to be able to predict any changes in marine productivity as deoxygenated
193 regions grow. This study contributes towards this goal through examining four open research
194 questions in OMZ biogeochemistry:

195 (1) Is the rapid cycle hypothesis correct, i.e., that NO_3^- reduction and NO_2^- oxidation rates are
196 much greater than N loss rates, especially in the oxycline and ODZ top?

197 (2) Does truly anaerobic NO_2^- oxidation occur in OMZ regions?

198 (3) If yes, is NO_2^- dismutation the mechanism by which it occurs?

199 (4) Is anammox the dominant N loss flux? If yes, what is the explanation?



200

201 **Figure 1:** Sampling locations during 2018 cruises to the ETNP OMZ. SR1805 stations (spring
202 2018) are shown in yellow while FK180624 (summer 2018) stations are shown in cyan. Stations
203 PS1 and 18 are located in more oxic environments on the boundary of the OMZ region. The
204 remaining FK180624 stations occur along a gradient towards the center of the OMZ region,
205 represented by stations PS2 and FK180624 stations 2 and 3. These three stations are referred to
206 as OMZ core stations. Station PS3 (referred to as coastal) represents a final biogeochemical
207 subregion due to its proximity to the coast.

208

209 **2. Methods**

210 **2.1 NO_2^- , NO_3^- , and NH_4^+ concentration measurements**

211 Nutrient measurements on all cruises were conducted as follows. Ambient NO_2^-
212 concentrations were measured on each vessel using the sulfanilimide and NED colorimetric
213 technique with a spectrophotometer (Strickland and Parsons, 1972). NO_3^- profile samples were
214 frozen onboard each ship, then thawed and measured immediately using the chemiluminescence
215 method upon return to the Ward laboratory (Braman and Hendrix, 1989). Ambient NH_4^+
216 concentrations were measured on each ship using the OPA method (Holmes et al., 1999; Taylor
217 et al., 2007; ASTM International, 2006). In some cases, NO_2^- and NH_4^+ were measured on
218 different casts than those of the rate measurements. In these cases, figures and calculations use
219 interpolated nutrient values based on the potential density of nutrient sampling and rate
220 measurement depths. Interpolations were performed with the Matlab `pchip` function.

221 **2.2 NH_4^+ oxidation and NO_3^- reduction rates**

222 Incubation experiments were performed on board the R/V *Sally Ride* in March and April
223 2018 (SR1805). NH_4^+ oxidation and NO_3^- reduction rates were measured at three stations: PS1
224 (open ocean OMZ boundary), PS2 (open ocean, OMZ), and PS3 (coastal OMZ) (Fig. 1). Rates
225 were measured throughout the water column at ten depths per station (see supplemental Table S1
226 for depths). Water was directly sampled from the CTD into 60 mL serum vials. After
227 overflowing three times, bottles were sealed with a rubber stopper and crimped with an

228 aluminum seal. After this, a 3 mL headspace of He was introduced and samples from below the
229 oxygenated surface depths were purged for 15 min with He at a flow rate of 0.4 L min⁻¹. This
230 flow rate exchanged the volume of each bottle one hundred times. Immediately after this, 0.1
231 mL of tracer solution was added to all bottles. ¹⁵NH₄⁺ and ¹⁵NO₃⁻ tracers were added to reach
232 final concentrations of 0.5 μM and 3 μM, respectively. Five bottles were incubated per time
233 course and incubations were ended at 0 (one bottle), 12, and 24 hours (two bottles each) via
234 addition of 0.2 mL of saturated ZnCl₂. Samples were analyzed at the University of Basel using a
235 custom-built gas bench connected by a Conflow IV interface to a Delta V plus IRMS (Thermo
236 Fisher Scientific). Five mL of the sample were used to convert NO₂⁻ to N₂O using the azide
237 method (McIlvin and Altabet, 2005). A linear increase of ¹⁵N-NO₂⁻ over time, along with a
238 standard curve to convert from peak area units to nmol N was used to calculate the NO₂⁻
239 production rates according to Eq. (5) and (6) below,

240 Ammonium oxidation rate = $\frac{d \text{ }^{15}\text{NO}_2^-}{dt (F_{\text{NH}_4^+})}$ (5)

241 Nitrate reduction rate = $\frac{d \text{ }^{15}\text{NO}_2^-}{dt (F_{\text{NO}_3^-})}$ (6)

242 where:

243 $\frac{d \text{ }^{15}\text{NO}_2^-}{dt}$ is the slope of ¹⁵NO₂⁻ produced over time and

244 F_{NH₄⁺} and F_{NO₃⁻} are the fraction of the NO₃⁻ and NH₄⁺ pools that are labelled with ¹⁵N.

245 The significance of the rates was evaluated using a Student's t test with a significance level of
246 0.05. The reported error bars are the standard error of the regression. The NH₄⁺ oxidation rates
247 reported here were previously published and the experimental method used is more thoroughly
248 described in this previous publication (Frey et al., 2022).

249

250 **2.3 Anammox and denitrification rates depth profiles**

251 Incubation experiments were performed during SR1805 in March and April 2018 and on
252 the R/V *Falkor* (FK180624) during June and July 2018. As above, rates were measured at PS1,
253 PS2, and PS3 at ten depths per station (see Supplementary Table S1 for sampling depths) during
254 SR1805. On FK180624, rates were measured at eight stations that spanned a gradient from the
255 core of the OMZ region to its edges (see Supplementary Table S2 for sampling depths). At all
256 stations and depths water was directly sampled from the CTD into 320 mL borosilicate ground
257 glass stoppered bottles. After overflowing three times, bottles were stoppered with precision
258 ground glass caps specifically produced to prevent gas flow. The bottles were transferred to a
259 glove bag and amended with the following treatments: 3 μM each of $^{15}\text{NO}_2^-$ and $^{14}\text{NH}_4^+$
260 (denitrification and anammox) and 3 μM each of $^{15}\text{NH}_4^+$ and $^{14}\text{NO}_2^-$ (anammox) on SR1805. 2
261 μM amendments of $^{15}\text{NO}_2^-$ and $^{14}\text{NH}_4^+$ were used on FK180624. It should be noted that at many
262 depths our tracer additions were far above in situ values. Due to this, all anammox and
263 denitrification rates with high changes from baseline nutrient concentrations represent potential
264 rates. Eight mL of tracer amended seawater was aliquoted into 12 mL exetainers (Labco).
265 Exetainers were sealed in a glove bag with butyl septa and plastic screw caps that had been
266 stored under helium for at least one month, removed and then purged for 5 min at 3 psi with
267 helium gas to remove any O_2 that accumulated during sampling and processing. This step is
268 another reason our anammox and denitrification rates sourced from partially or fully oxygenated
269 waters should be regarded as potential rates.

270 Rates for each sampled depth were calculated using a five-timepoint time course with
271 three replicates at each point. Incubations were ended by injecting 50 μL saturated ZnCl_2 and

272 vials were stored upside down to prevent the headspace from leaking through the vial cap during
 273 storage and transit. Six months after the cruise, samples were analyzed using a Europa 22-20
 274 IRMS (Sercon). Raw data values were corrected for instrument drift due to run position and
 275 total N₂ mass. Drift corrected values and standard curves to convert from peak area units to
 276 nmol N₂ were used to calculate rates according to the equations below (Thamdrup et al., 2006;
 277 Thamdrup and Dalsgaard, 2000, 2002) (for more details see supplemental material),

278 Denitrification (from ¹⁵NO₂⁻)

$$279 \text{ Denitrification Rate} = \frac{d \text{ }^{30}\text{N}_2}{dt(F_{\text{NO}_2^-})^2} \quad (7)$$

280 Anammox (from ¹⁵NO₂⁻)

$$281 \text{ Anammox Rate} = \frac{d \text{ }^{29}\text{N}_2}{dt F_{\text{NO}_2^-}} - 2D(1 - F_{\text{NO}_2^-}) \quad (8)$$

282 Anammox (from ¹⁵NH₄⁺)

$$283 \text{ Anammox Rate} = \frac{d \text{ }^{29}\text{N}_2}{dt F_{\text{NH}_4^+}} \quad (9)$$

284 where:

285 $\frac{d \text{ }^{30 \text{ or } 29}\text{N}_2}{dt}$ is the slope of the regression of the amount of ^{30 or 29}N₂ vs. time,

286 F_{NO₂⁻} and F_{NH₄⁺} are the fraction of the NO₂⁻ and NH₄⁺ pools labelled as ¹⁵N, and

287 *D* is the denitrification rate calculated according to Eq. (7).

288 A Student's *t* test with a significance level of 0.05 was used to evaluate all rates. The reported
 289 error bars are the standard error of the regression. Since the anammox rates measured via both
 290 tracers on the SR1805 cruise were similar in magnitude (Supplementary Table S3), anammox
 291 values reported in Figs. 2, 3, 6, 7, 8, and 9 are based on a combination of these values (see

292 supplementary material for more information). Previously published (Babbin et al., 2020)
293 anammox and denitrification rates are sourced from four stations occupied during the R/V
294 *Thomas G. Thompson*'s March and April 2012 cruise to the ETNP (TN278) and the RVIB
295 *Nathaniel B. Palmer*'s June and July 2013 ETSP cruise (NBP1305) and were conducted in the
296 same manner as the SR1805 and FK180624 incubations. Crucially, the same mass spectrometer
297 was used to measure N loss rates across the 2012, 2013, and 2018 cruises. Station locations for
298 the 2012 and 2013 cruises were as follows: TN278 ETNP coastal (20° 00' N, 106° 00' W),
299 ETNP offshore (16° 31' N, 107° 06' W) and NBP1305 ETSP coastal (20° 40' S, 70° 41' W),
300 ETSP offshore (13° 57' S, 81° 14' W).

301

302 **2.4 SR1805 NO₂⁻ oxidation depth profiles**

303 Nitrite oxidation depth profiles were measured in the same exetainers used to measure
304 anammox and denitrification depth profiles (¹⁵NO₂⁻ treatment only). The rate of NO₂⁻ oxidation
305 was determined by converting the NO₃⁻ produced during the incubations to N₂O using the
306 denitrifier method (Weigand et al., 2016; Granger, J., & Sigman, 2009) (see supplemental
307 material for methods details). The samples were stored at room temperature in the dark until
308 analysis on a Delta V (Thermo Fisher Scientific) mass spectrometer that measures the isotopic
309 content of N in N₂O (Weigand et al., 2016). Samples were corrected for instrument drift due to
310 run position and total N₂ mass (for more details see supplemental materials). Drift corrected
311 δ¹⁵N values and a standard curve were then used to calculate the rate as follows,

$$312 \frac{^{15}\text{N}}{^{14}\text{N}} = \frac{\left[\frac{\delta^{15}\text{N}}{1000} + 1 \right] \times 0.003667}{1 - 0.003667} \quad (10)$$

313
$$\text{NO}_2^- \text{ ox. rate} = \frac{d \left[{}^{44}\text{N}_2\text{O}_{\text{area}} \times \frac{{}^{15}\text{N}}{{}^{14}\text{N}} \right]}{dt F_{\text{NO}_2^-}} \quad (11)$$

314 where Eq. (10) is a rearrangement of the definition of $\delta^{15}\text{N}$:

315
$$\delta^{15}\text{N} = \left[\frac{\frac{{}^{15}\text{N}}{{}^{14}\text{N}}_{\text{sample}}}{\frac{{}^{15}\text{N}}{{}^{14}\text{N}}_{\text{air}}} - 1 \right] \times 1000 \quad (12)$$

316 and ${}^{44}\text{N}_2\text{O}_{\text{area}}$ is the amount of ${}^{44}\text{N}_2\text{O}$ measured as sample peak area in $\text{V} \cdot \text{sec}$. 0.003667 is the
 317 natural abundance of ${}^{15}\text{N}$ in air. A Student's t test with a significance level of 0.05 was used to
 318 evaluate all rates. Reported error bars are the standard error of the regression. Previously
 319 published (Babbin et al., 2020) NO_2^- oxidation rates are from the previously mentioned TN278
 320 and NBP1305 cruises and were conducted at the same four stations where N loss rates were
 321 measured. These NO_2^- oxidation rate measurements were conducted according to the same
 322 procedures used for the SR1805 depth profiles.

323

324 **2.5 NO_2^- oxidation and O_2 manipulation experiments**

325 Experiments were conducted during cruises SR1805 and FK180624 in spring and
 326 summer 2018. Wide-mouthed Pyrex round media bottles (800 mL total volume, 500 mL
 327 working volume; Corning, USA; product code 1397-500) were used for all incubations. These
 328 bottles were modified to include three stainless steel bulkhead fittings (Swagelok, USA) secured
 329 to the interior of the lid with a Viton rubber gasket and stainless-steel washer between the lid and
 330 the sealing nut. The three ports consisted of two one-eighth inch fluidic ports (inflow and
 331 outflow) and one one-quarter inch sampling port. The fluidic ports were fitted with one-eighth
 332 inch nylon tubing, with the inflow line penetrating to the base of the bottle. The one-quarter inch

333 sampling port had a butyl rubber septum between the Swagelok stem and nut. This setup
334 permitted *continuous* gas purging of the bottles while maintaining an otherwise closed system.

335 For each depth and O₂ treatment, three bottles were filled to 500 mL with sample water
336 from a Niskin bottle and closed. Sample water for all experiments except station 18 on the
337 FK180624 cruise was drawn from water below 2.2 μM O₂ (See Table S4 for all ambient O₂
338 values). Highly precise digital mass flow controllers (Alicat) were then used to establish the
339 desired O₂ concentrations in each bottle. Mixing ratios were calculated to create a range of O₂
340 concentrations spanning 1 nM, 10 nM, 100 nM, 1 μM, and 10 μM. The gas mixture modified by
341 the mass flow controllers was a zero-air gas mixture (Airgas) consisting of 21% O₂ and 79% N₂
342 and 1000 ppm pCO₂ (the approximate in situ value). Initial gas flow was 1 L min⁻¹ for 1 hour to
343 equilibrate the seawater followed by 100 mL min⁻¹ for the remainder of the experiment. Bottles
344 were daisy-chained together to maintain the same flow rate among them (two bottles on SR1805,
345 six on FK180624). As in the depth profile experiments, 3 μM ¹⁵NO₂⁻ amendments were added
346 prior to purging. Incubations were conducted in the dark at 12°C in a cold room (SR1805) or
347 beverage cooler (FK180624). At the beginning of the experiments, after purging for one hour,
348 O₂ was checked with a LUMOS optode with a detection limit of 0.5 nM (Lehner et al., 2015) and
349 CO₂ was checked by measuring pH using the colorimetric meta-cresol purple method. The
350 LUMOS optode confirmed that O₂ concentrations were within a few nM of the calculated values.
351 While our use of high precision digital mass flow controllers and this qualitative O₂ check
352 provide confidence that our O₂ concentrations are accurate, due to the fact that O₂ was not
353 continuously monitored through the time course, we refer to each O₂ concentration as a
354 “putative” concentration for the remainder of this manuscript. Samples (50 mL) were withdrawn
355 every 12 hours for two days with a four inch hypodermic needle attached to a 60 mL disposable

356 plastic syringe. Samples were ejected into acid-cleaned HDPE bottles pre-amended with 200 μL
357 of saturated ZnCl_2 solution. Bottles were screwed closed and wrapped with parafilm. Samples
358 from each of the three initially collected bottles were collected to create triplicates at each time
359 point.

360

361 **2.6 NO_2^- dismutation experiments**

362 Nitrite dismutation experiments were performed during SR1805 at Station PS3 (coastal
363 waters) at two deoxygenated depths: 60 m and 160 m. Incubations were performed in the same
364 manner as the above anammox, denitrification, and NO_2^- oxidation experiments where all three
365 rates were measured in the same exetainers. Experiments consisted of eight total treatments:
366 four varying $^{15}\text{NO}_2^-$ tracer concentrations (1.125, 5.25, 10.5, and 20.25 μM for 160 m and 0.75,
367 1.5, 3.75, and 7.5 μM for 60 m) and two $^{14}\text{NO}_3^-$ treatments (0 or 20 μM). As above, both $^{30}\text{N}_2$
368 and NO_3^- production via the denitrifier method (Weigand et al., 2016) were measured. In order
369 to test our hypothesis that, if dismutation is occurring, the unexplained NO_2^- oxidation rate (the
370 difference between the measured NO_2^- oxidation and the NO_2^- oxidation due to anammox) and
371 the denitrification rate (i.e. the $^{30}\text{N}_2$ production rate) should have a 3:1 ratio, a previously
372 published anammox stoichiometry (Eq. (4) (Kuenen, 2008)) was used to calculate the NO_2^-
373 oxidation due to anammox. The anammox rates used for this calculation are included in the
374 supplementary material (Fig. S4).

375

376 **2.7 Calculation of N loss from NH_4^+ oxidation**

377 The calculation of the maximum possible N loss from NH_4^+ oxidation via NO
378 disproportionation by ammonium oxidizing archaea (AOA) in Supplementary Table S5 was

379 carried out by dividing the measured NH_4^+ oxidation rate by two in accordance with the
380 stoichiometry of NH_4^+ oxidation and NO disproportionation proposed in a previous study (Kraft
381 et al., 2022). It should be noted that this operation represents the extreme case where all $^{15}\text{NO}_2^-$
382 produced in NH_4^+ oxidation is converted to N_2 . We acknowledge this as an unrealistic
383 assumption used to evaluate the extreme limits of the amount of total N loss attributable to NH_4^+
384 oxidation. This operation was carried out for all depths where NH_4^+ oxidation, anammox, and
385 denitrification rates were measured, irrespective of O_2 concentration.

386

387 **2.8 Redundancy analysis (RDA), Principle component analysis (PCA), and statistics**

388 All RDA, PCA, redundancy, and correlation analyses were performed with the available
389 packages in R (v4.2.1 “Funny-Looking Kid”) (R: A language and environment for statistical
390 computing). All data were first normalized around zero before calculating the Pearson’s
391 correlation coefficient. Gene abundances (*nirS* and *amoA*) from qPCR analyses used for the
392 RDA and correlation analyses were measured as previously described (Peng et al., 2015;
393 Jayakumar et al., 2009; Tang et al., 2022).

394

395 **2.9 Definition of shallow boundary and ODZ core nomenclature**

396 In the results and discussion sections, results are classified as shallow boundary or ODZ
397 core waters according to a previously published threshold (Babbin et al., 2020) where shallow
398 boundary samples have an in situ potential density < 26.4 . This method is based on a global
399 profile of OMZ waters meant to delineate shallow boundary samples as waters that are oxic or
400 may be influenced by O_2 intrusions (the surface, the oxycline, and the ODZ top) from those that
401 are not normally influenced by O_2 intrusions (ODZ core). Due to the fact that the potential

402 density threshold is based on a global average, a few depths that are clearly in the deep oxycline
 403 based on the SR1805 O₂ depth profiles are classified as ODZ core ($\sigma_{\theta} > 26.4$) by the potential
 404 density threshold. Despite this caveat we used this naming scheme throughout the remainder of
 405 the manuscript to enable comparisons to previous literature (Babbin et al., 2020).

Depth	σ_{θ}	OMZ features	O ₂ intrusions?
Shallow boundary waters	< 26.4	Surface, oxycline, ODZ top	Yes
ODZ core	> 26.4	ODZ core	No

406
 407 **Table 1:** Explanation of shallow boundary waters and ODZ core potential density based
 408 nomenclature (Babbin et al., 2020).
 409

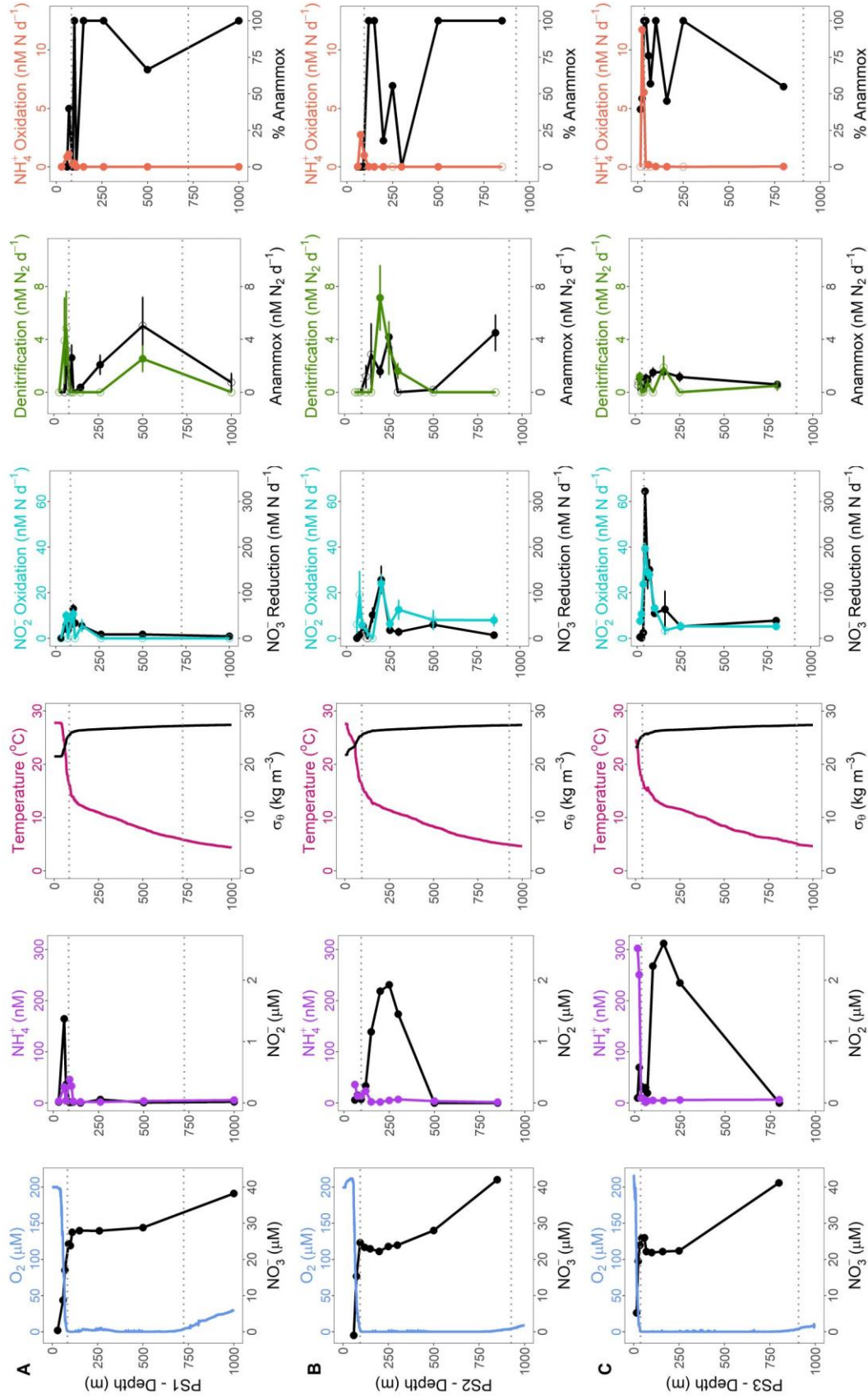
410 3. Results

411 3.1 2018 depth profiles of all N cycling rates

412 N cycling depth profile experiments were conducted on two cruises (SR1805 and
 413 FK180624) during spring and summer 2018. These two cruises sampled stations along a
 414 gradient from the edge of the OMZ region to near the coast. Physical and chemical conditions
 415 varied among stations PS1, PS2, and PS3 on the SR1805 cruise (spring 2018) and across all
 416 FK180624 stations (summer 2018) (Fig. 2, Fig. S1). Broadly speaking, the vertical span of the
 417 ODZ increased and the top of the ODZ shoaled as distance to shore decreased. Deep SNM were
 418 observed at almost all stations with the only exceptions being the furthest offshore stations,
 419 stations 11 and 18 from the FK180624 cruise (Fig. S1) and station PS1 from SR1805 (Fig. 2A).
 420 Peak NO₂⁻ values for all SNM were on the lower side of the range of previous ETNP
 421 observations (Horak et al., 2016), between 1.4 – 2.6 μ M.

422 Of the five N cycling processes measured on the SR1805 cruise, NO₃⁻ reduction rates had
 423 the greatest magnitude at most depths. This trend was most pronounced within the upper ODZ,
 424 where NO₃⁻ reduction rates peaked at station PS2, and the oxycline where NO₃⁻ reduction rates

425 peaked at stations PS1 and PS3 (Fig. 2). Rates of NO_2^- oxidation closely tracked NO_3^- reduction
426 in distribution; in fact, peak NO_2^- oxidation rates co-occurred with peak NO_3^- reduction rates at
427 all three SR1805 stations, reaching maxima of ~ 40 (NO_2^- oxidation) and ~ 300 (NO_3^- reduction)
428 nM N d^{-1} at PS3. However, the magnitudes of NO_2^- oxidation rates were usually lower than
429 NO_3^- reduction rates, sometimes by as much as eightfold. The third N recycling process, NH_4^+
430 oxidation, peaked at or above the oxycline, with peaks of 10 nM N d^{-1} or less. NH_4^+ oxidation
431 was consistently measured to be zero or near-zero throughout the rest of the water column.
432



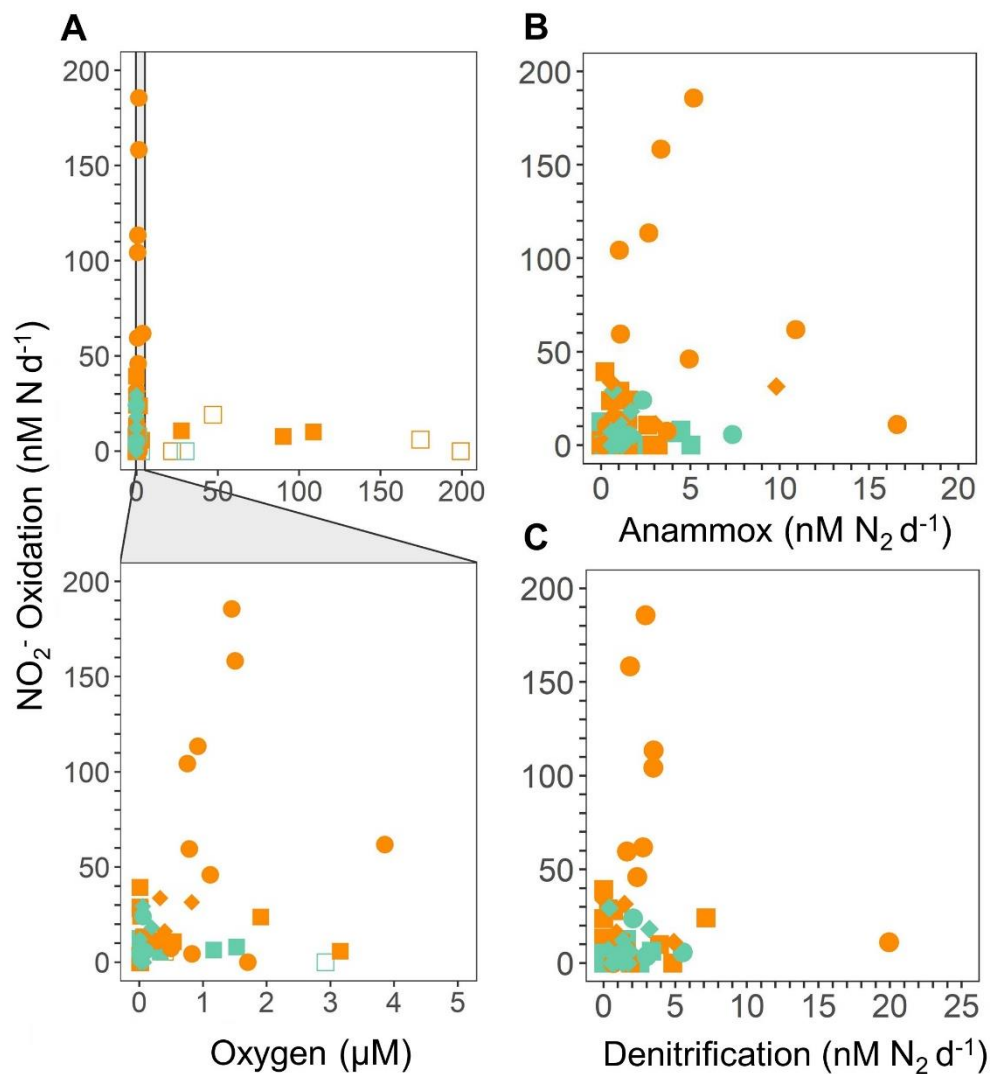
434 **Figure 2:** SR1805 depth profiles of physical parameters and N cycling rates. **(A)** From left to
435 right, O₂ (μM) and NO₃⁻ (μM) respectively in blue and black, NH₄⁺ (nM) and NO₂⁻ (μM)
436 respectively in purple and black, temperature (°C) and σ_θ (kg m⁻³) respectively in pink and black,
437 NO₂⁻ oxidation and NO₃⁻ reduction rates (nM N d⁻¹) respectively in cyan and black, anammox
438 and denitrification rates (nM N₂ d⁻¹) respectively in black and green, NH₄⁺ oxidation rates (nM
439 N d⁻¹), and percent anammox respectively in coral and black for station PS1 (offshore). **(B)** As
440 above but for station PS2 (OMZ). **(C)** As above but for station PS3 (coastal). Rates that are
441 significantly different from zero are shown as filled circles, open circles signify rates not
442 significantly different from zero. Error bars are the standard error of the regression. Grey dotted
443 lines indicate upper and lower ODZ boundaries at the time of sampling.
444

445 Across all SR1805 and FK180624 stations, the magnitude of the N loss processes of
446 anammox and denitrification was almost always less than 10 nM N₂ d⁻¹, a much lower magnitude
447 than the N recycling processes of NO₃⁻ reduction and NO₂⁻ oxidation. Like NO₃⁻ reduction and
448 NO₂⁻ oxidation, the two N loss rates peaked in the upper ODZ or right at the oxycline in all three
449 SR1805 stations, although a deep peak (850 m) in anammox was observed at station PS2 (Fig.
450 2B). This peak occurred near the bottom of the ODZ at an O₂ concentration of 1.5 μM. N loss
451 rates also peaked near the oxycline in the three FK180624 stations with broad coverage of the
452 ODZ water column, stations 2, 9 (6 July sampling), and 9 (9 July sampling) (Fig. S1). The
453 relative balance between the two N loss processes as measured by percent anammox varied
454 widely across the water column but largely deviated from the expected partitioning of at most
455 29% anammox (Dalsgaard et al., 2003, 2012). A striking example of this is that 100% anammox
456 values were observed in both ODZ core and shallow boundary (see Table 1 for definitions)
457 samples at many of the SR1805 and FK180624 stations (Fig. 2, Fig. S1).
458

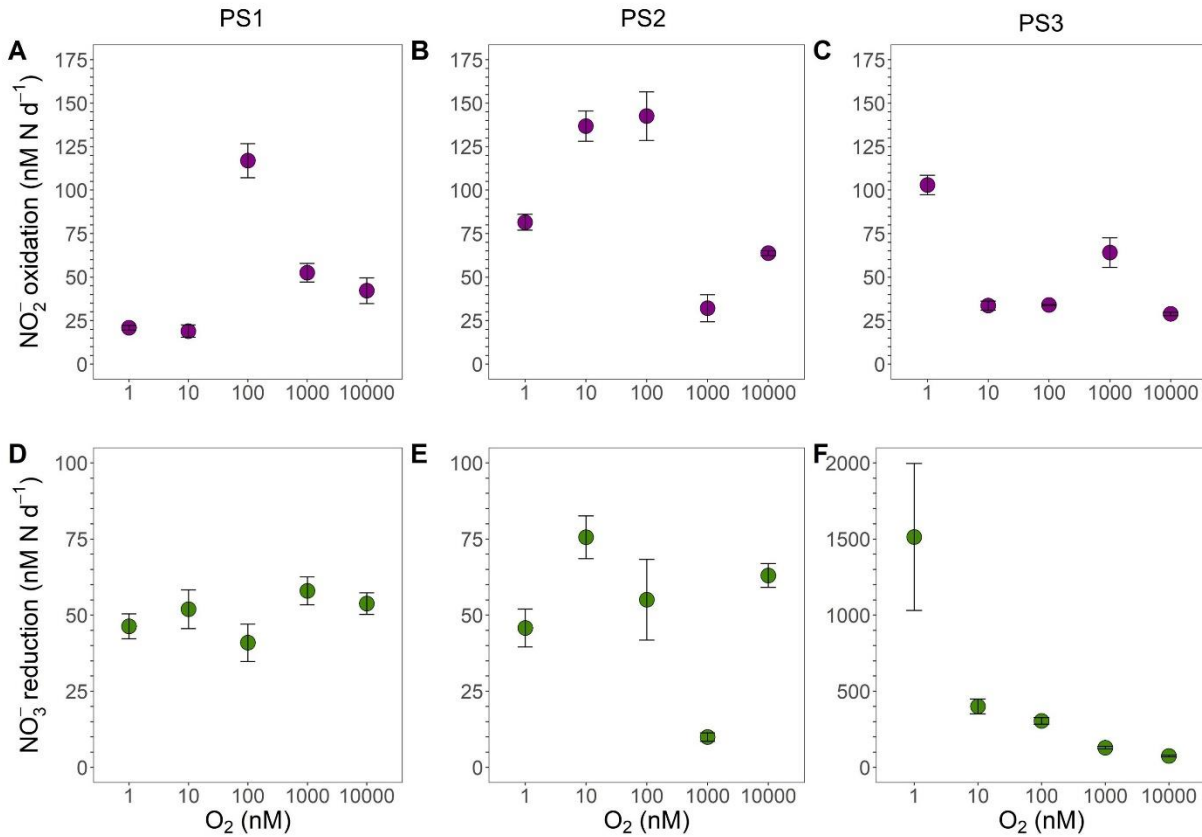
459 **3.2 Anaerobic NO₂⁻ oxidation and O₂ manipulation experiments**

460 Significant NO₂⁻ oxidation rates were detected in depth profiles across a range of suboxic
461 O₂ concentrations (1 – 5 μM) (definition from (Berg et al., 2022)) across all SR1805 stations,
462 often at the same depths and in the same vials where the obligately anaerobic processes of

463 anammox and denitrification were occurring (Fig. 2, Fig. 3A-C, Fig. S2). In order to
464 contextualize our observations, we compared our results to previously published measurements
465 from the TN278 and NBP1305 cruises performed with identical procedures (Babbin et al., 2020).
466 The highest rates were observed in shallow boundary waters across all three cruises (Fig. 3A-C,
467 Fig. S2). Since low but significant levels of O₂ can still support aerobic NO₂⁻ oxidation, a series
468 of O₂ manipulation experiments was carried out on both the SR1805 (spring) and FK180624
469 (summer) 2018 cruises (Fig. 4A-F and Fig. S3). In these experiments, anoxic conditions were
470 checked using a LUMOS O₂ optode with a detection limit of 0.5 nM (Lehner et al., 2015). We
471 observed significant NO₂⁻ oxidation, as well as NO₃⁻ reduction at putative concentrations as low
472 as 1 nM. Notably, compared to previous experiments, gas flushing was constant, with a refresh
473 time of 8 min, so as to maintain O₂ levels within the incubation even while organisms were
474 respiring. At 1nM, O₂ is so scarce that such waters are usually classified as functionally anoxic,
475 for example, a recent review paper defined 3 nM as the threshold below which O₂ cannot play
476 biological or biogeochemical roles (Berg et al., 2022). As a result, these experiments present
477 convincing additional evidence for the occurrence of NO₂⁻ oxidation up to ~100 nM N d⁻¹ at O₂
478 concentrations too low to support aerobic metabolisms.
479



480
 481
 482 **Figure 3:** NO_2^- oxidation rates (nM N d^{-1}) from the 2018 SR1805 (squares), 2012 ETNP TN278
 483 (circles), and 2013 ETSP NBP1305 (diamonds) cruises vs. (A) O_2 concentration (μM) from
 484 shipboard CTD sensors, (B) anammox rates ($\text{nM N}_2 \text{d}^{-1}$), and (C) denitrification rates ($\text{nM N}_2 \text{d}^{-1}$).
 485 O_2 concentrations were normalized across cruises. In A, rates that are significantly different
 486 from zero as assessed via a Student T-test (p value < 0.05) are displayed as filled symbols, while
 487 insignificant NO_2^- oxidation rates are shown as open symbols. Rates measured in shallow
 488 boundary waters are colored orange while rates from the ODZ core and below are colored teal.
 489 2012 and 2013 data are republished (Babbin et al., 2020).
 490



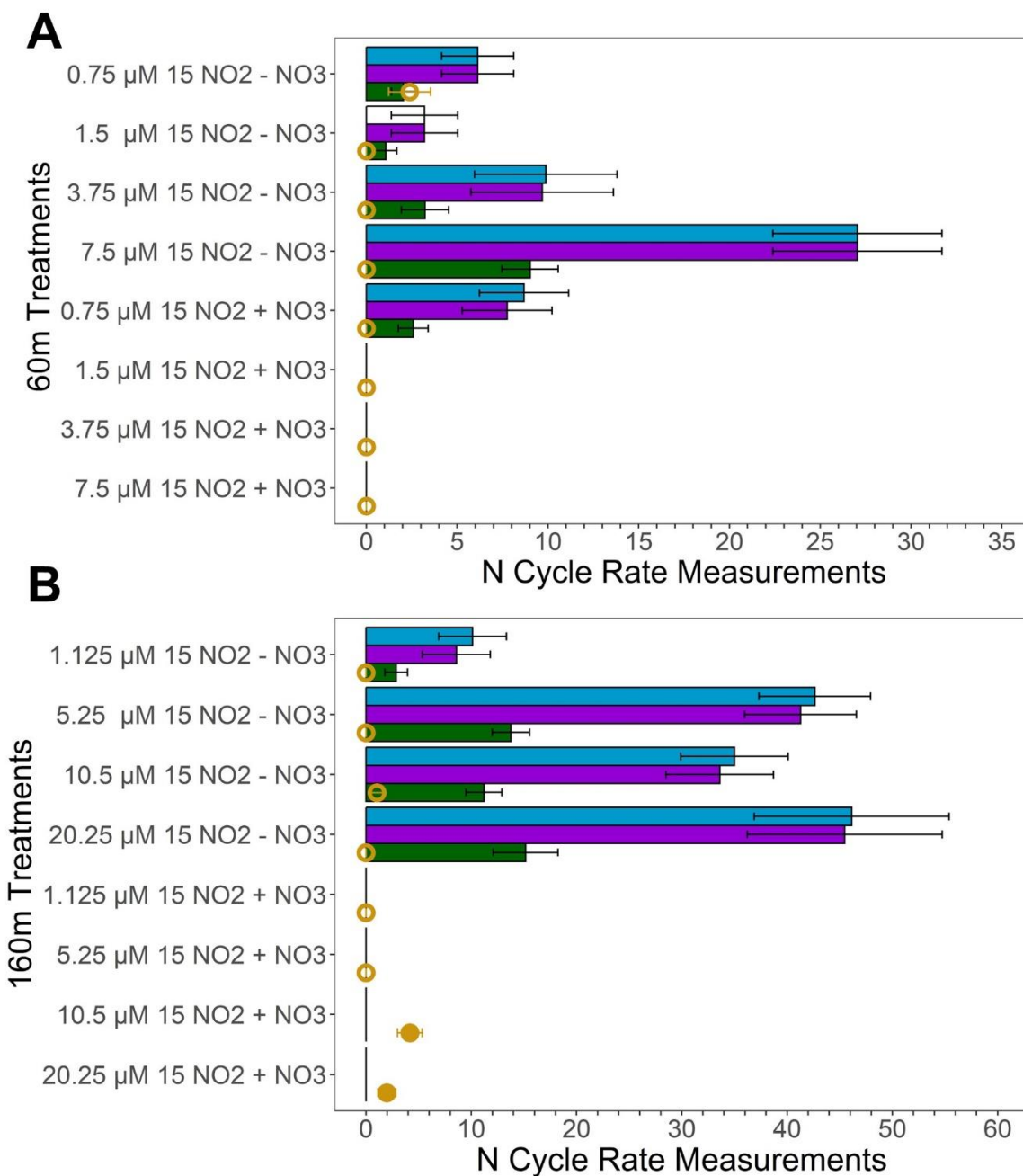
491
 492
 493 **Figure 4:** Oxygen manipulation experiments that show NO_2^- oxidation (purple) (A-C) and NO_3^-
 494 reduction (green) (D-F) rates (nM N d^{-1}) measured across putative O_2 concentrations from 1 to
 495 10,000 nM during the SR1805 cruise. Experiments were conducted with waters from the ODZ
 496 top: 93 – 110m (PS1) (A, D), 113 – 130m (PS2) (B, E), and 45 – 60m (PS3) (C, F). Error bars
 497 are the standard error of the regression. All rates were significantly different from zero.

498
 499 **3.3 NO_2^- dismutation**

500 In order to investigate the mechanism for the observed anaerobic NO_2^- oxidation,
 501 experiments were conducted to search for evidence of NO_2^- dismutation. If NO_2^- dismutation is
 502 the dominant explanation for the observed anaerobic NO_2^- oxidation, we hypothesized that (1)
 503 adding NO_3^- should suppress both $^{30}\text{N}_2$ and NO_3^- production by LeChatelier’s principle, (2)
 504 increasing $^{15}\text{NO}_2^-$ concentration should increase both denitrification (the $^{30}\text{N}_2$ production rate)
 505 and NO_2^- oxidation especially when no additional NO_3^- was added, and (3) that the ratio
 506 between the “unexplained NO_2^- oxidation,” i.e., the difference between the observed NO_2^-

507 oxidation and the NO_2^- oxidation due to anammox, and the observed denitrification ($^{30}\text{N}_2$
508 production) rate should be close to 3:1. In experiments with He-purged water from two
509 deoxygenated depths (60 and 160 m at station PS3, see table S5 for O_2 values) during the
510 SR1805 cruise we observed that adding 20 μM NO_3^- suppressed NO_2^- oxidation across nearly all
511 pairs of 0 and 20 μM NO_3^- experiments where the NO_2^- concentration was identical (Fig. 5).
512 However, we did not observe a simultaneous suppression of N_2 production due to the fact that
513 the measured denitrification rate was low and insignificantly different from zero in most of our
514 16 treatments (Fig. 5). The lack of an observed response in N_2 production could be due to
515 already elevated ambient NO_3^- concentrations, 26 μM and 22.2 μM at 60 m and 160 m
516 respectively. Roughly doubling the amount of NO_3^- would have little effect on the
517 denitrification rate if the relevant enzymes were already saturated, as is plausible at those
518 concentrations. As a result of our inability to observe denitrification, our first hypothesis yielded
519 little evidence of dismutation.

520 Across all four 60 m 0 μM added NO_3^- treatments (Fig. 5A), adding NO_2^- did increase
521 NO_2^- oxidation; however, we did not observe an increase in denitrification. Surprisingly, across
522 the four 60 m 20 μM added NO_3^- treatments, adding NO_2^- decreased NO_2^- oxidation, the reverse
523 of our hypothesis (Fig. 5). Across all four 160 m 0 μM added NO_3^- treatments, we also observed
524 an increase in NO_2^- oxidation at higher NO_2^- concentrations but did not observe an increase in
525 the measured denitrification rate (Fig. 5B). In the four 160 m 20 μM added NO_3^- treatments,
526 NO_2^- oxidation and denitrification did not increase with NO_2^- concentration (Fig. 5B). Due to
527 the consistently low and insignificant denitrification rates our test of the NO_2^- addition
528 hypothesis also yielded little evidence for dismutation.



529

530 **Figure 5:** NO_2^- dismutation tests conducted in deoxygenated waters from 60m (**A**) and
 531 at station PS3 during the SR1805 cruise. Measured NO_2^- oxidation rates (nM N d^{-1}) are
 532 displayed in blue, unexplained NO_2^- oxidation rates, the difference between the measured NO_2^-
 533 oxidation and the NO_2^- oxidation due to anammox (nM N d^{-1}), are shown in purple. The
 534 predicted denitrification ($\text{nM } ^{30}\text{N}_2 \text{ d}^{-1}$) if all the unexplained NO_2^- oxidation was due to NO_2^-
 535 dismutation is shown in green. The measured denitrification rate ($\text{nM } ^{30}\text{N}_2 \text{ d}^{-1}$) is shown in
 536 yellow where filled circles indicate significant rates and open circles indicate rates that are not
 537 significantly different from zero. All bars filled with colors indicate significant rates (i.e. the
 538 white bar for the 60 m 1.5 μM $^{15}\text{NO}_2^-$, 0 μM NO_3^- treatment NO_2^- oxidation rate denotes an

539 insignificant rate). Error bars are the standard error of the regression for NO_2^- oxidation, or are
540 calculated based on the rules of error propagation from the standard error of the regressions for
541 the NO_2^- oxidation and anammox rates. (+) NO_3^- treatments received $20 \mu\text{M } ^{14}\text{NO}_3^-$ additions
542 while the (-) NO_3^- treatments received no addition. Anammox rates used to calculate the
543 unexplained NO_2^- oxidation rate are shown in the supplementary material.

544
545 We were also unable to observe evidence for the ratio hypothesis due to the paucity of
546 significant denitrification ($^{30}\text{N}_2$ production) rates (Fig. 5). Since denitrification rates were
547 consistently low or insignificantly different from zero, the ratio of NO_2^- oxidation to
548 denitrification deviated from the 3:1 ratio expected if NO_2^- dismutation accounts for most of the
549 observed NO_2^- oxidation. The only slight exception to this is the 60 m treatment with $0.75 \mu\text{M}$
550 $^{15}\text{NO}_2^-$ and $0 \mu\text{M}$ added NO_3^- , the treatment closest to in situ conditions. In this treatment, the
551 measured denitrification rate, while insignificantly different from zero on the basis of the p value
552 of the regression, agrees with the predicted denitrification rate based on the 3:1 stoichiometry of
553 dismutation. While our dismutation experiments as a whole suggest that NO_2^- dismutation is not
554 a likely explanation for observed anaerobic NO_2^- oxidation, results from the 60 m $0.75 \mu\text{M}$
555 $^{15}\text{NO}_2^-$, $0 \mu\text{M}$ NO_3^- treatment provide slight justification to continue tests of this hypothesis.

556

557 **4. Discussion**

558 **4.1 Rapid $\text{NO}_2^- / \text{NO}_3^-$ cycle**

559 Depth profiles of N transformation rates obtained on the SR1805 cruise show that the
560 rates of NO_2^- oxidation and NO_3^- reduction are far greater than rates of the N loss processes of
561 anammox and denitrification, especially in shallow boundary (see Table 1 for definition) waters
562 (Fig. 2, Fig. 6A – B). In fact, when the combined N recycling pathways of NO_2^- oxidation and
563 NO_3^- reduction are compared to the total N loss, the N recycling pathways are 3.2 – 192.8 times
564 larger than the total N loss. That the minimum ratio is ~ 3 strongly emphasizes the

565 preponderance of NO_2^- oxidation and NO_3^- reduction above N loss processes. As expected due
566 to the oligotrophic nature of the offshore ETNP (Fuchsman et al., 2019) and as previously found
567 in an ETSP N cycling study (Kalvelage et al., 2013), NO_2^- oxidation and NO_3^- reduction
568 generally increased from the offshore station (PS1) towards the coast. We observed NO_3^-
569 reduction rates of a similar magnitude to previously reported ETSP studies (Kalvelage et al.,
570 2013; Babbin et al., 2017), a finding that generalizes the predominance of NO_3^- reduction to
571 NO_2^- to the ETNP. Thus, our work supports several recent studies (Babbin et al., 2020, 2017;
572 Peters et al., 2016) suggesting that most nitrogen within OMZ regions is continuously recycled
573 between NO_2^- and NO_3^- by rapid NO_2^- oxidation and NO_3^- reduction, especially in shallow
574 boundary waters.

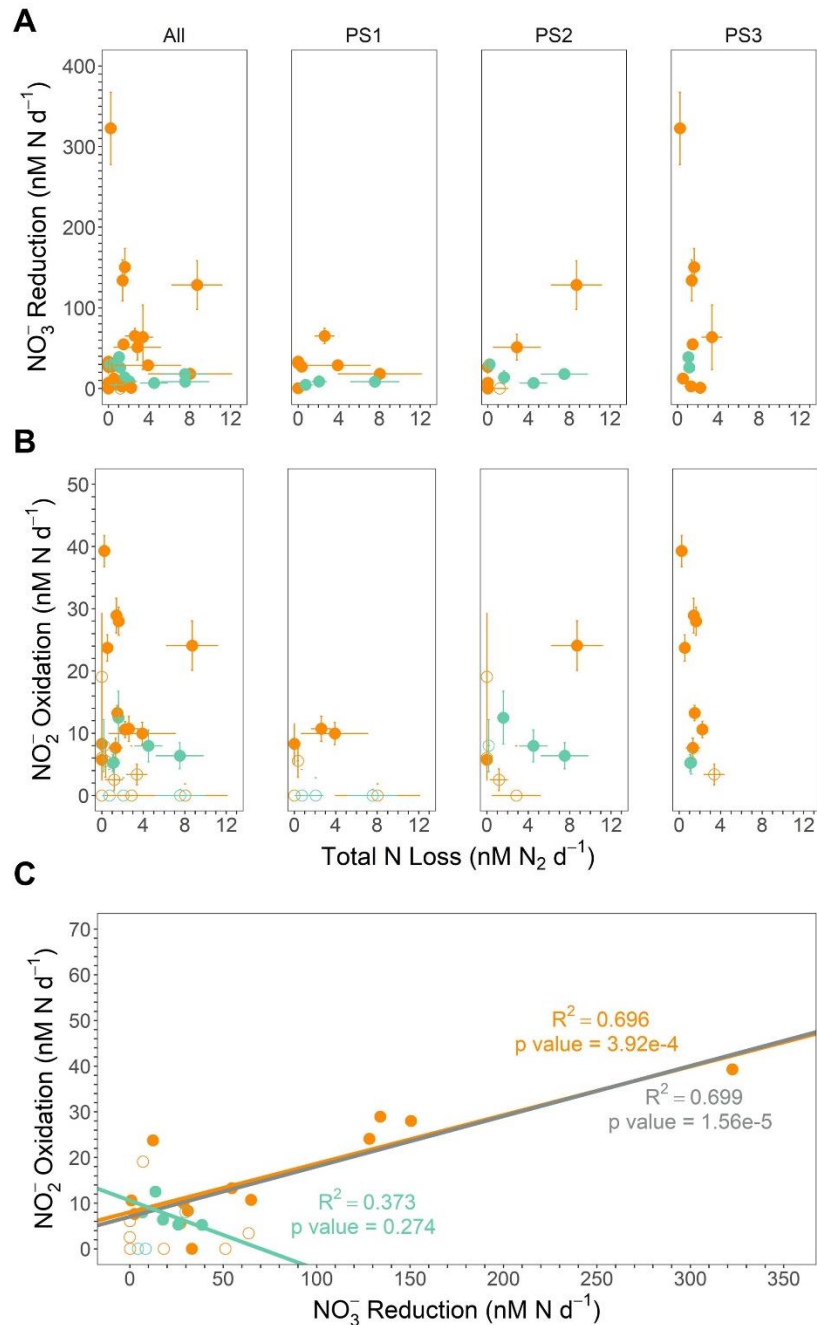
575 A previous work (Babbin et al., 2017) predicted that NO_3^- reduction should follow a
576 Martin curve (Martin et al., 1987) power law distribution across the water column due to its
577 dependence on the OM flux from shallower waters. Such a distribution was observed at stations
578 PS1 and PS3; however, NO_3^- reduction at station PS2 did not follow a classical Martin curve
579 profile since the NO_3^- production peak is well below the oxycline. This exception could be due
580 to zooplankton which have been observed to migrate into the ODZ on a daily basis (Bianchi et
581 al., 2014). Due to the fact that migrating zooplankton funnel surface OM to the mesopelagic
582 (Cram et al., 2022), such a transfer would move OM in a pattern not consistent with the Martin
583 curve. The transferred OM could then support the observed peak in NO_3^- reduction (Fig. 2).

584 These results are consistent with the idea, also supported by many recent studies
585 (Kalvelage et al., 2013; Lam and Kuypers, 2011; Lam et al., 2009; Babbin et al., 2020, 2017;
586 Füssel et al., 2011; Lam et al., 2011), that the accumulated NO_2^- in the SNM usually results from
587 an imbalance between NO_3^- reduction and other N cycling pathways. We further investigated

588 this hypothesis by constructing a net NO_2^- budget derived from the five microbial N cycling
589 metabolisms measured on the SR1805 cruise (Fig. 7). Summing the depth profiles of NO_2^-
590 consumption (anammox, denitrification, and NO_2^- oxidation) and production (NH_4^+ oxidation
591 and NO_3^- reduction) pathways revealed that net depth integrated NO_2^- production across the
592 sampled OMZ water column depths is on the order of tens of millimoles of NO_2^- per square
593 meter per day at all three stations (8.19 at PS1, 14.49 at PS2, and 28.97 $\text{mmol NO}_2^- \text{ m}^{-2} \text{ d}^{-1}$ at
594 PS3). This excess NO_2^- is driven by NO_3^- reduction, which across all stations is of a much
595 greater magnitude than all other measured N cycling processes (Fig. 2 and Fig. 7).

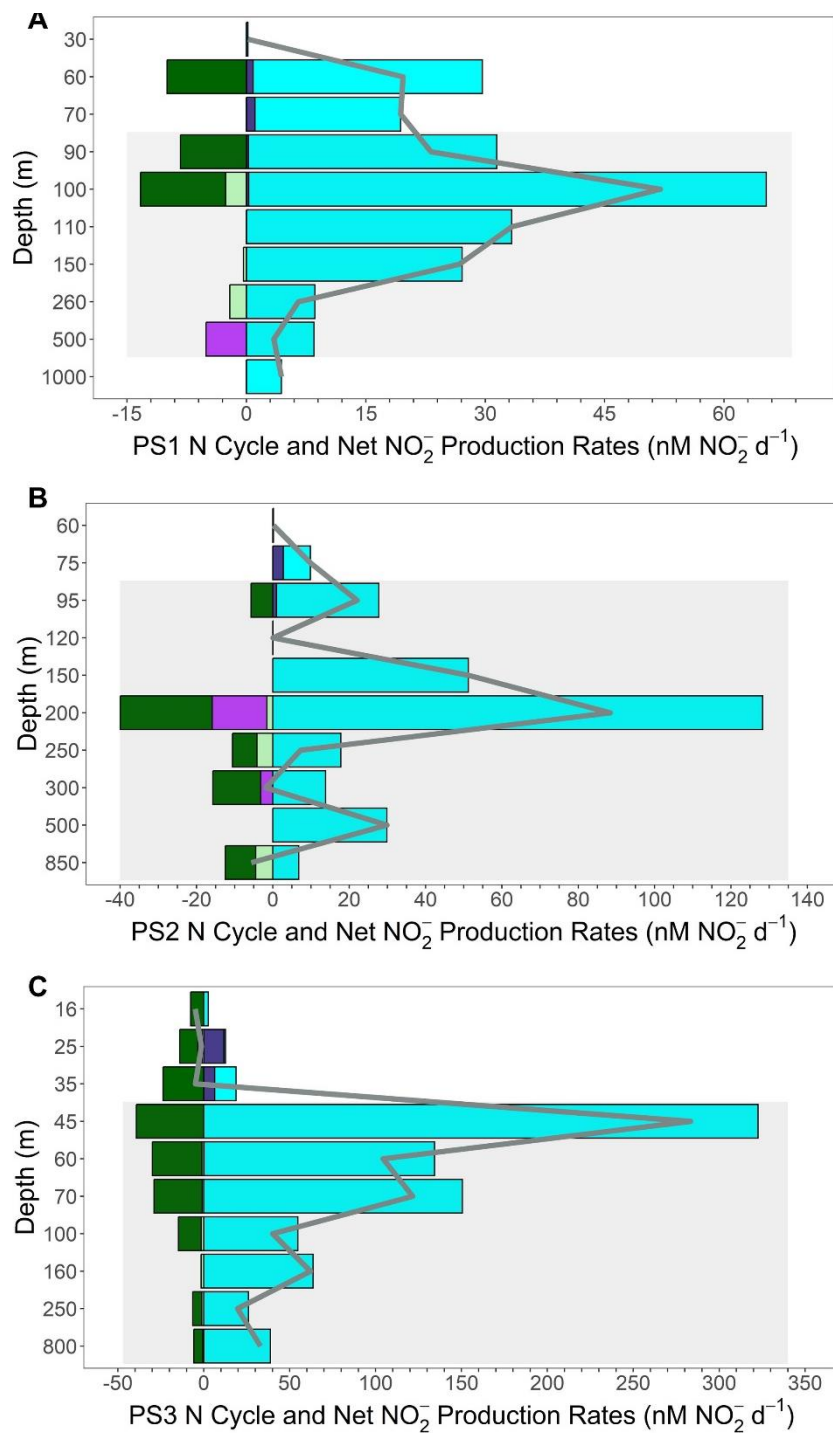
596 These budget calculations take the reported rates at face value, ignoring the likelihood
597 that some of them are potential rates. For example, anammox might have been enhanced by the
598 addition of 3 $\mu\text{M NH}_4^+$. Denitrification is less likely to be stimulated by the addition of NO_2^-
599 because it is generally limited by organic matter availability (Ward et al. 2008, Babbin et al
600 2014). Thus, the relative importance of anammox and denitrification might be perturbed due to
601 differential responses of the two rates to tracer additions. Analogously, NO_2^- oxidation was
602 likely stimulated by addition of NO_2^- tracer (Sun et al. 2017), but NO_3^- reduction less so by
603 addition of NO_3^- tracer because the latter is a heterotrophic process, and as a component of the
604 complete denitrification pathway, likely limited by organic matter availability. These differential
605 limitations by substrate probably mean that the calculated budget of Figure 7 is not completely
606 accurate, but the relative importance of the processes is robust. If anything, the dominance of
607 anammox over denitrification is probably less than that observed, and the excess of NO_3^-
608 reduction over NO_2^- oxidation greater than observed. Overall, the dominance of the $\text{NO}_3^- / \text{NO}_2^-$
609 loop over the N loss pathways and the overwhelming importance of NO_3^- reduction are both
610 supported by these considerations.

611 Additional support that NO_3^- reduction supplies the accumulated NO_2^- in the SNM can
612 be found by comparing the net NO_2^- production rates with the measured NO_2^- concentrations
613 along the SR1805 cruise track from offshore station PS1 to coastal station PS3. As would be
614 expected if the SNM depended on NO_2^- derived from NO_3^- reduction, the peak net NO_2^-
615 production value across all depths at each station, the depth integrated NO_2^- production values
616 for each station, and the magnitude of the SNM peak NO_2^- concentrations all increase together
617 from offshore station PS1 to coastal station PS3. Importantly, we did not take into account water
618 column mixing in both vertical and horizontal directions that would carry away produced NO_2^-
619 or NO_2^- assimilation into OM, and we recommend follow up studies that include
620 parameterizations for these values in OMZ N Cycling modeling.



621

622 **Figure 6:** (A) NO_3^- reduction (nM N d^{-1}) vs. Total N loss (the sum of denitrification and
 623 anammox in $\text{nM N}_2 \text{d}^{-1}$) from the SR1805 cruise. (B) NO_2^- oxidation (nM N d^{-1}) vs. Total N loss
 624 from the SR1805 cruise. (C) NO_2^- oxidation vs. NO_3^- reduction. Regression lines and statistics
 625 are shown for the significant rates from shallow boundary waters only (orange), ODZ core
 626 waters only (teal), and all significant data (grey). All points from shallow boundary waters are
 627 colored orange while all points from the ODZ core or below are colored teal. Open circles
 628 indicate points where the NO_3^- reduction rate (A), NO_2^- oxidation rate (B), or in (C) either NO_3^-
 629 reduction or NO_2^- oxidation rate is not significantly different from zero while filled circles
 630 indicates rates significantly different from zero.

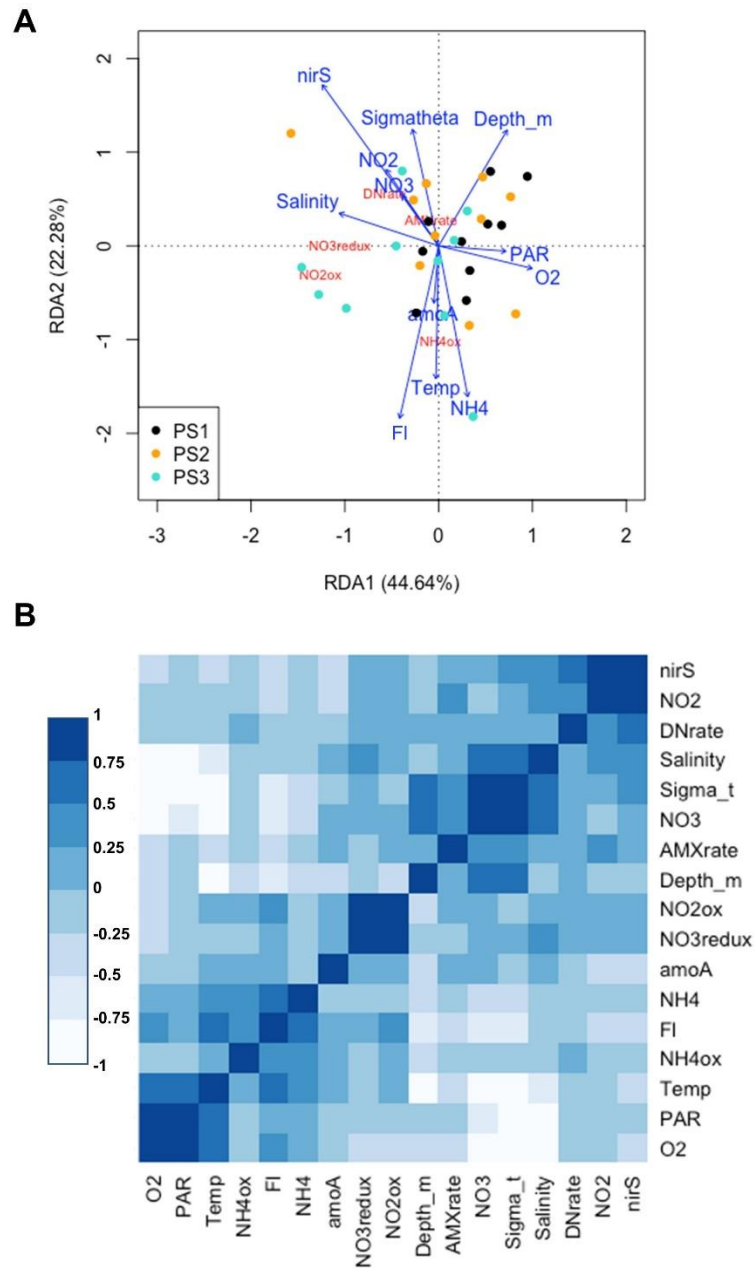


631
632

633 **Figure 7:** NO_2^- budget profiles from the SR1805 cruise. Plots are a combination of the NO_2^-
634 production pathways of NO_3^- reduction (cyan), NH_4^+ oxidation (dark purple) and the NO_2^-
635 consumption pathways of anammox (light green), denitrification (bright purple), and NO_2^-
636 oxidation (dark green). Consumption pathways are reported as negative numbers. All rates are
637 reported in $\text{nM NO}_2^- \text{d}^{-1}$. The net NO_2^- production or consumption rate ($\text{nM NO}_2^- \text{d}^{-1}$) is
638 represented as a grey line for each depth. Grey boxes indicate the completely deoxygenated
639 ODZ region at each station at the time of sampling. (A) PS1, (B) PS2, and (C) PS3.

640 4.2 NO₂⁻ oxidation – distribution and magnitude in comparison to previous studies

641 The high rates of observed NO₃⁻ reduction provide sufficient NO₂⁻ to support NO₂⁻
642 oxidation both in the oxycline and in the ODZ, as previously proposed (Anderson et al., 1982),
643 Our observations also further confirm isotopic studies that suggested high NO₂⁻ oxidation rates
644 because rapid re-oxidation of NO₂⁻ back to NO₃⁻ was necessary to achieve isotopic mass balance
645 (Buchwald et al., 2015; Casciotti et al., 2013; Granger and Wankel, 2016). Our results also align
646 with previous experimental observations of high NO₂⁻ oxidation rates (Kalvelage et al., 2013;
647 Babbin et al., 2020; Lipschultz et al., 1990). Support for a closely connected rapid cycle
648 between the two processes can be seen in the strong correlation between NO₂⁻ oxidation and
649 NO₃⁻ reduction observed in all SR1805 cruise samples, especially those from shallow boundary
650 waters (Fig. 6C, Fig. 8). Similarly to some previous ETSP papers (Babbin et al., 2017, 2020;
651 Frey et al., 2020) and two ETNP studies (Peng et al., 2015; Sun et al., 2017) we observed that
652 rates of NO₂⁻ oxidation, like rates of NO₃⁻ reduction, peaked in the oxycline or in the ODZ top
653 (Fig. 2) and then declined throughout the ODZ. Unlike some stations in these studies (Babbin et
654 al., 2020, 2017) we did not observe a second peak in NO₂⁻ oxidation near the deep oxycline. In
655 addition to observing a similar distribution, we also observed that NO₂⁻ oxidation occurs at a
656 similar magnitude to some stations in previous ETSP studies (Babbin et al., 2020, 2017; Peng et
657 al., 2016) and ETNP (Peng et al., 2015), although our highest rates (25 – 40 nM N d⁻¹) were
658 much lower than the peaks measured at other stations in most of these reports (Babbin et al.,
659 2020; Peng et al., 2015, 2016), which reached as high as ~600 nM N d⁻¹ (Peng et al., 2015;
660 Lipschultz et al., 1990).



661

662 **Figure 8:** (A) Redundancy analysis of all environmental variables and microbial rates measured
 663 on the SR1805 cruise. Points are color-coded by station, black (PS1), yellow (PS2), and cyan
 664 (PS3). Variables names and arrows are color coded so that environmental variables are blue and
 665 rate measurements are red. (B) Correlation analysis for all environmental variables and
 666 microbial N cycle rates from the SR1805 cruise. More positive correlations are shaded to
 667 become bluer as significance grows while negative correlations are shaded to become whiter as
 668 significance grows. Abbreviations used are as follows: O2 (oxygen concentration normalized
 669 across different sensors), PAR (photosynthetically active radiation normalized across sensors),
 670 NH4ox (NH₄⁺ oxidation rate), FI (chlorophyll fluorescense normalized across different sensors),
 671 NH4 (NH₄⁺ concentration), *amoA* (*amoA* abundance), NO3redux (NO₃⁻ reduction rate), NO2ox

672 (NO_2^- oxidation rate), AMXrate (anammox rate), NO3 (NO_3^- concentration), DNrate
673 (denitrification rate), NO2 (NO_2^- concentration), and *nirS* (*nirS* abundance).

674

675

676 **4.3 NO_2^- oxidation – can it occur anaerobically?**

677 NO_2^- oxidation depth profiles (Figs. 2, 3) and O_2 manipulation experiments (Fig. 4)

678 provide further evidence that NO_2^- oxidation can occur even when O_2 is as low as ~ 1 nM. .

679 While our O_2 manipulation experiments provide the most convincing evidence of anaerobic

680 NO_2^- oxidation, several factors argue that the NO_2^- oxidation observed in our depth profile

681 incubations may be O_2 independent. As argued previously (Babbin et al., 2020):

682 (1) The pre-incubation He purging step in our depth profile method removes more than 99% of

683 the N_2 present in exetainers (Babbin et al., 2020). If it is assumed that O_2 is removed at identical

684 efficiency, a reasonable proposition since O_2 equilibrates faster than N_2 (Wanninkhof, 1992), the

685 introduction during sample processing of as much as $1 \mu\text{M}$ O_2 would result in a ~ 10 nM

686 contamination. As a result, if NO_2^- oxidation is observed in samples from the deoxygenated ODZ

687 core, contamination during sampling would be kept very small by our purging step. This

688 conclusion was further validated by direct O_2 measurements using Lumos sensors in exetainers.

689 These tests of our purging method showed that O_2 was reduced to less than 10 nM in 5 minutes

690 (Sun et al. unpublished data).

691 (2) Linear timecourses across all timepoints were observed in some of our experiments,

692 including many from deoxygenated depths at station PS3 (Supplemental Figs. S7-9). If NO_2^-

693 oxidation depended on O_2 , an initial acceleration (due to O_2 contamination that sparked NO_2^-

694 oxidation) or later steep drop (due to the exhaustion of O_2 by aerobic NOB) in NO_2^- oxidation

695 would be expected, not a consistent linear slope.

696 (3) Metagenomic evidence has revealed distinct NOB communities in oxic surface waters, the
697 oxycline and ODZ top, and the ODZ core in OMZ regions (Sun et al., 2019). In addition we
698 observed decreasing NO_2^- oxidation rates with increasing in situ O_2 in the SR1805 incubations as
699 well as the TN278 and NBP1305 incubations (Fig. 3A). These observations are consistent with
700 the hypothesis that aerobic NOB from oxic depths are ill-equipped to oxidize NO_2^- in
701 deoxygenated conditions but that the unique MAGs recently identified in draft genomes from the
702 ODZ top and core (Sun et al., 2019), are adapted to perform anaerobic NO_2^- oxidation.

703 (4) Through plotting O_2 concentrations against the ratio between NO_3^- reduction and NO_2^-
704 oxidation at all SR1805 depths with significant, positive NO_2^- oxidation rates, we observed that
705 the known anaerobic process of NO_3^- reduction and NO_2^- oxidation did not exhibit differential
706 regulation by O_2 as would be expected if NO_2^- oxidation was an obligately aerobic process (Fig.
707 S5).

708 Previous studies have shown that O_2 additions to purged incubations of ODZ waters can
709 inhibit NO_2^- oxidation (Sun et al., 2017, 2021a) and that NO_2^- oxidation can occur in the absence
710 of O_2 consumption (Sun et al., 2021a). However, another kinetics study has reported O_2
711 stimulation of NO_2^- oxidation in OMZ waters (Bristow et al., 2016) and concluded that NO_2^-
712 oxidation is fundamentally an aerobic process. This apparent contradiction might be explained
713 by several details in the experimental process of that study (Bristow et al., 2016):

714 (1) The study site is at the farthest edge of the ETSP OMZ in a location that is only anoxic in the
715 austral summer.

716 (2) The cruise was conducted as austral summer turned to fall (March 20 – 26th), a period where
717 O_2 intrusions would be more likely.

718 (3) O₂ data from the study's cruise (Tiano et al., 2014) show that the depths from which NO₂⁻
719 oxidation O₂ kinetics samples were sourced experienced O₂ concentrations of 2 μM (50 m), 10
720 μM (40 m), and > 60 μM (30m) either during sampling or a few days prior to sampling.
721 As a result, we argue that the observed stimulation of NO₂⁻ oxidation by O₂ (Bristow et al., 2016)
722 occurred not because all OMZ NOB are aerobic NO₂⁻ oxidizers, but instead because the location,
723 season, and levels of O₂ of the sampled station selected for aerobic NOB in the source water for
724 the purged incubations. Thus, as suggested by (Sun et al., 2017, 2021a), different NOB
725 populations with different historical exposures to O₂ and adaptations likely respond differently to
726 O₂ manipulations.

727 Here we built on the above previous tests of anaerobic NO₂⁻ oxidation by conducting a
728 series of incubations across an O₂ gradient from ~1 nM to 10 μM. Site waters for these
729 incubations were drawn from the ODZ top at each SR1805 station (Table S4). We did not
730 observe a clear inhibitory or stimulatory response of NO₂⁻ oxidation to O₂ within the SR1805 or
731 FK180624 stations; however, this lack of a clear response is in itself a revealing result - a lack of
732 consistent stimulation by O₂ implies at least some anaerobic NOB were present. In addition, we
733 consistently observed significant NO₂⁻ oxidation at all putative O₂ concentrations, including 1
734 nM, a concentration usually considered functionally anoxic. Since the O₂ in the incubations was
735 continuously supplied by a mass flow controller and subsequently checked via an extremely
736 sensitive O₂ sensor for all incubations, these results provide additional evidence that truly
737 anaerobic NO₂⁻ oxidation can occur.

738 One argument against our characterization of the NO₂⁻ oxidation observed at ~1 nM O₂
739 as functionally anoxic is that the K_m of NO₂⁻ oxidation has been calculated to be as low as 0.5
740 nM (Bristow et al., 2016). However, the data used to calculate this value have the same

741 qualifications discussed previously: (1) the study site is at a location only anoxic during the
742 austral summer, (2) the cruise was conducted during a time when O₂ intrusions would be more
743 likely, and (3) the sampled waters experienced O₂ concentrations as high as 60 μM prior to
744 sampling. Such conditions would favor aerobic NOB and the expression of high affinity NO₂⁻
745 oxidation enzymes by these organisms when exposed to low O₂ conditions in incubations. As a
746 result, we argue that the modeled K_m value of 0.5 nM only applies when NOB with higher O₂
747 niches are placed in sub-micromolar O₂ conditions. This value does not apply to NOB observed
748 to prefer ODZ conditions (Sun et al., 2019), which we assume would be favored under our 1 nM
749 treatment.

750 These O₂ manipulation experiments also provided an opportunity to investigate the
751 response of NO₃⁻ reduction to O₂. The only clear intra-station pattern that emerged from these
752 experiments was that at station PS3, NO₃⁻ reduction displayed possible inhibition by O₂, as
753 would be expected. Due to the small number of data points in our data set we did not attempt a
754 kinetics fitting for this data. Interestingly, the disparity observed in depth profile experiments
755 between the magnitudes of the NO₃⁻ reduction and NO₂⁻ oxidation rates was not observed in the
756 O₂ manipulations across many O₂ concentrations at stations PS1 and PS2. At station PS3 a large
757 disparity in the magnitudes of these processes as well as the highest overall NO₃⁻ reduction rates
758 were observed, as in the depth profile experiments (Fig. 4, 7). A few of the FK180624 data
759 points also exhibited NO₃⁻ reduction rates that were elevated far above NO₂⁻ oxidation (Fig. S3).
760 These results confirm the importance of NO₃⁻ reduction for the rapid recycling cycle as well as
761 the source of NO₂⁻ for the SNM.

762

763 **4.4 NO₂⁻ dismutation**

764 In the absence of O_2 , NO_2^- oxidation would require another oxidant. Many candidate
765 oxidants have been suggested. For example, iodate (IO_3^-), an abundant marine species with
766 global average marine concentrations of $\sim 0.5 \mu M$ (Nozaki, 1997; Lam and Kuypers, 2011), has
767 been proposed and shown to stimulate NO_2^- oxidation (Babbin et al., 2017). However, since
768 IO_3^- is usually absent within the ODZ core (Moriyasu et al., 2020), its low concentration makes
769 IO_3^- mediated anaerobic NO_2^- oxidation in that location unlikely (Babbin et al., 2020). NO_2^-
770 oxidation via Mn^{4+} or Fe^{3+} is thermodynamically feasible, but only at low pH (< 6) (Luther, 2010;
771 Luther and Popp, 2002). This pH constraint, combined with the fact that concentrations of these
772 ions are on the order of a few nM in OMZs (Kondo and Moffett, 2015; Vedamati et al., 2015),
773 makes these mechanisms unrealistic for the ODZ core. Another proposed mechanism is that the
774 observed NO_2^- oxidation is due to anammox, which if true should result in an observed NO_2^-
775 oxidation to anammox ratio of 0.16 – 0.3 (Kuenen, 2008; Strous et al., 1998; Oshiki et al., 2016).
776 Instead, the observed ratio is sometimes more than 10x this range and NO_2^- oxidation is rarely
777 observed to be less than anammox (Kalvelage et al., 2013; Babbin et al., 2020; Sun et al., 2021a).

778 Another alternative hypothesis is based on the reversibility of the nitrite oxidoreductase
779 (NXR) enzyme. Since this enzyme has been suggested to both oxidize NO_2^- and reduce NO_3^-
780 (Kemeny et al., 2016; Koch et al., 2015; Wunderlich et al., 2013), NO_3^- reduction by NXR could
781 over time enrich the ^{15}N - NO_3^- pool since lighter $^{14}NO_3^-$ would be favored (Casciotti, 2009).
782 Even in $^{15}NO_2^-$ tracer experiments, in which the NO_2^- pool is highly labeled, this reversibility at
783 the enzyme site could lead to an apparent transfer of ^{15}N from the NO_2^- to the NO_3^- pool if NXR
784 mediated NO_3^- reduction was occurring. This hypothesis is supported by observations of NO_3^-
785 reduction under low O_2 in cultures from the NOB genera *Nitrobacter* (Freitag et al., 1987; Bock
786 et al., 1990), *Nitrospira* (Koch et al., 2015), and in pure cultures of *Nitrococcus mobilis* (Füssel

787 et al., 2017). In addition, a recent study presented natural abundance isotopic evidence in pure
788 *Nitrococcus mobilis* cultures consistent with this mechanism (Buchwald and Wankel, 2022).

789 However, NXR reversibility has not been demonstrated for the abundant (Füssel et al.,
790 2011; Mincer et al., 2007) and sometimes dominant (Beman et al., 2013) OMZ NOB genera
791 *Nitrospina*. Furthermore, the sole source of the isotopic evidence for the enzyme reversibility
792 hypothesis, *Nitrococcus mobilis*, has a cytoplasm facing NXR substrate binding domain
793 (Buchwald and Wankel, 2022), a feature found to have an established evolutionary relationship
794 to NAR (the known NO_3^- reductase enzyme family) in other *Nitrobacter* studies (Starkenbourg et
795 al., 2008; Kirstein and Bock, 1993). The NXR substrate binding domains in *Nitrospina* are
796 oriented towards the periplasm and are not evolutionarily related to enzymes for NO_3^- reduction
797 (Buchwald and Wankel, 2022; Sun et al., 2019). Due to these structural and phylogenetic
798 differences among NOB NXR, it is possible that the *Nitrospina* NXR may be unable to perform
799 NO_3^- reduction as easily as other NOB genera. For all these reasons, it is not yet clear if the
800 enzyme reversibility hypothesis can explain all NO_2^- oxidation measured under low O_2
801 conditions and other hypotheses should continue to be explored.

802 As a result of the above proposals' shortcomings, this paper focused on the remaining,
803 most plausible hypothesis: NO_2^- dismutation. Our tests for dismutation rested on three
804 hypotheses: (1) that NO_3^- additions would inhibit both NO_2^- oxidation and $^{30}\text{N}_2$ production by
805 LeChatelier's principle, (2) that increasing $^{15}\text{NO}_2^-$ should energetically favor dismutation,
806 especially in treatments with no additional NO_3^- , and (3) that the ratio of non-anammox
807 mediated NO_2^- oxidation to denitrification ($^{30}\text{N}_2$ production) should be close to 3:1 if NO_2^-
808 dismutation explains most of the observed NO_2^- oxidation. We observed repeated inhibition of
809 NO_2^- oxidation by NO_3^- but no inhibition of $^{30}\text{N}_2$ production due to the fact that denitrification

810 was consistently low and insignificantly different from zero across all treatments. In treatments
811 with 0 μM added NO_3^- , increasing NO_2^- generally increased NO_2^- oxidation, but not
812 denitrification. In addition, the ratio of anammox corrected NO_2^- oxidation to observed
813 denitrification deviated from dismutation's 3:1 stoichiometry in almost all treatments. However,
814 we did observe simultaneous inhibition of N_2 and NO_3^- production as well as good agreement
815 between the anammox corrected NO_2^- oxidation / denitrification ratio to the NO_2^- dismutation
816 stoichiometry in one treatment - the treatment most similar to in situ conditions (60m, 0.75 μM
817 $^{15}\text{NO}_2^-$, 0 μM NO_3^-). As a result, while our results show little evidence for dismutation overall,
818 we recommend additional experiments at tracer levels similar to 0.75 μM $^{15}\text{NO}_2^-$ to further test
819 for NO_2^- dismutation.

820

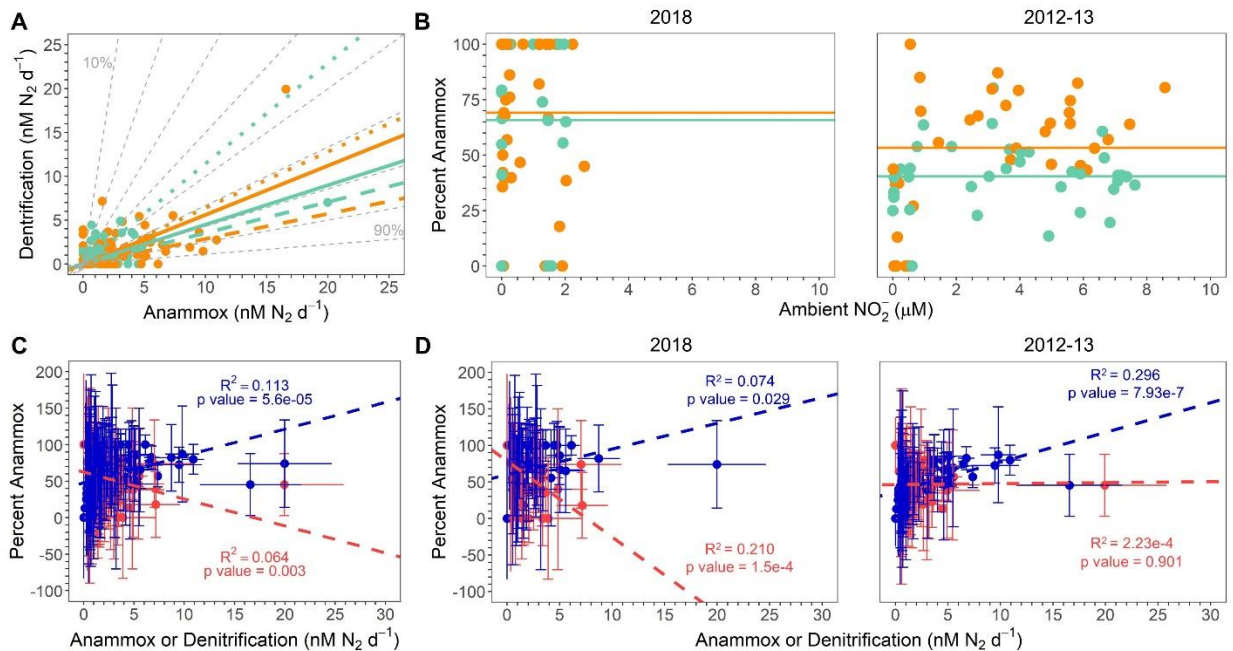
821 **4.5 Relative balance of anammox and denitrification**

822 **4.5.1 Are results consistent with past observations of slow, low, and steady anammox** 823 **elevated above the predicted maximum of 29% of total N loss?**

824 According to predictions based on the composition of average marine OM (Dalsgaard et
825 al., 2003, 2012) anammox should account for at most 29% of the total N loss flux in OMZ
826 regions. To test this hypothesis under a variety of conditions, regressions of denitrification vs.
827 anammox rates were calculated for all samples from the SR1805, FK180624, TN278, and
828 NBP1305 cruises. In order to compare our new data to a previous study (Babbin et al., 2020),
829 which observed variations in the ratio of anammox and denitrification between samples from the
830 ODZ top or above ($\sigma_\theta < 26.4$, "shallow boundary waters," (Babbin et al., 2020)) and samples
831 from the deoxygenated ODZ core or below ($\sigma_\theta > 26.4$, "ODZ core," (Babbin et al., 2020)),
832 regressions for all data (ODZ core), all data (shallow boundary), 2018 only (ODZ core), 2018

833 only (shallow boundary), 2012-13 (TN278, and NBP1305) only (ODZ core), and 2012-13 only
834 (shallow boundary) were calculated (Table S6). All regressions deviated from the predicted 29%
835 maximum anammox contour, although the regression from the 2012-13 cruises' ODZ core
836 samples was closest to the 30% anammox contour (Fig. 9A). We observed large differences in
837 the percent anammox contours near 2012-13 and 2018 regressions. ODZ core samples from
838 2012-13 regressed onto a line between the 40 and 50% anammox contours while ODZ core
839 samples from 2018 regressed onto a line between the 70% and 80% anammox contours.
840 Differences in contouring were smaller for the shallow boundary samples, although the 2018
841 samples still regressed to a higher contour (just under 80%) than the 2013-13 samples (60%)
842 (Fig. 9A). Our observations that all year and density based regressions fell within contours well
843 above the theoretical prediction (Fig. 9A) and that anammox accounted for as much as 100% of
844 the total N loss at many depths in 2018 samples (Fig. 2, Fig. 9B) is consistent with the many
845 previous studies that observed anammox as the predominant OMZ N loss pathway (Lam et al.,
846 2009; Thamdrup et al., 2006; Kuypers et al., 2005; Hamersley et al., 2007; Jensen et al., 2011).

847 Our new 2018 results do not contradict the idea (Dalsgaard et al., 2012) that anammox is
848 often measured to be the bulk of total N loss but that large, episodic occurrences of denitrification
849 can dwarf the consistent albeit low anammox contribution to total N loss. Under this view, these
850 eruptions in denitrification return the *time integrated* balance of anammox and denitrification to
851 its expected 29 and 71% values. In this scenario, our cruises' sampling, like many but not all
852 others, did not coincide with episodic high rates of denitrification.



853

854 **Figure 9:** (A) All 2012, 2013, and 2018 denitrification and anammox rates ($\text{nM N}_2 \text{d}^{-1}$), color-
 855 coded by σ_θ . ODZ core samples and lines are teal ($\sigma_\theta > 26.4$) while shallow boundary samples
 856 and lines are orange ($\sigma_\theta < 26.4$). Solid, dashed, and dotted lines respectively show regressions
 857 for all data, 2018 only, and 2012-13 data only. Dashed grey lines depict contours for percent
 858 anammox values. See Supplementary Table S6 for regression statistics. (B) Percent anammox
 859 vs. ambient NO_2^- for 2018 samples (left) and republished 2012 and 2013 samples (Babbin et al.,
 860 2020) (right). Points are colored according to the same scheme as panel A. Lines show the
 861 average percent anammox values in shallow boundary waters (orange) and the deoxygenated
 862 ODZ core (teal). (C) Percent anammox vs. all anammox (blue) and all denitrification (red)
 863 rates ($\text{nM N}_2 \text{d}^{-1}$). Regression lines shown for % AMX vs. anammox and denitrification rates follow
 864 the same color scheme as the data points. Error bars represent the standard error of the
 865 regression. (D) Percent anammox vs. anammox (blue) and denitrification (red) rates ($\text{nM N}_2 \text{d}^{-1}$)
 866 for 2018 only (left) and 2012-13 (right). Points and regression lines follow the same color
 867 scheme as in panel C. Data shown in the 2012-13 only panel are republished (Babbin et al.,
 868 2020).

869

870

871 4.5.2 Do results support a connection between rapid NO_3^- reduction and elevated

872 anammox?

873 Our 2018 results question the previously proposed view (Babbin et al., 2020) that rapid

874 NO_3^- reduction produces NH_4^+ that in turn elevates anammox in oxycline and upper ODZ

875 waters. While our data (Fig. 2) did find high rates of NO_3^- reduction in shallow boundary

876 waters, the 2018 N loss data do not show elevated shallow boundary (as compared to ODZ core)
877 percent anammox values as would be expected if high NO_3^- reduction were fueling elevated
878 anammox in the oxycline and ODZ top. This difference between our 2018 data and some
879 previous data (Babbin et al., 2020) in support of a connection between rapid NO_3^- reduction and
880 elevated anammox in the oxycline and ODZ top can be seen through a comparison of shallow
881 boundary ($\sigma_\theta < 26.4$ (Babbin et al., 2020)) and ODZ core ($\sigma_\theta > 26.4$ (Babbin et al., 2020)) percent
882 anammox values in the 2018 SR1805 and FK180624 cruises against the 2012-13 TN278 and
883 NBP1305 cruises (Fig. 9B). 2012-13 samples showed a clear partitioning between the ODZ core
884 and shallow boundary waters in terms of percent anammox values. In 2012-13, as would be
885 expected if high oxycline and ODZ top NO_3^- reduction were supplying NH_4^+ to anammox,
886 shallow boundary samples have a higher average percent anammox value than ODZ core
887 samples (Fig. 9B). In 2018, this partitioning was not present - the difference between the
888 average percent anammox values in ODZ core and shallow boundary samples was much smaller
889 (Fig. 9B). Interestingly, the total number of samples found to be 100% anammox also sharply
890 diverged between 2012-13 and 2018. In the 2012-13 samples, only one shallow boundary
891 sample was found to be 100% anammox. In 2018, many samples from both shallow boundary
892 waters and the ODZ core were 100% anammox (Fig. 9B, Fig. S6).

893 These observed differences in the partitioning of anammox and denitrification between
894 shallow boundary waters and the ODZ core across different years and places do not support the
895 view that NH_4^+ from rapid NO_3^- reduction of oxycline and ODZ top OM always elevates
896 anammox rates. Instead, they suggest that other factors play an important role in setting the
897 balance of anammox and denitrification. Interestingly, NO_2^- concentrations spanned a much
898 narrower range in the two 2018 SR1805 and FK180624 cruises than the 2012-13 TN278 and

899 NBP1305 cruises (Fig. 9B), a clue that the biogeochemical environment of the OMZ is subject to
900 interannual variability. Observed differences in environmental variables like NO_2^- and percent
901 anammox partitioning between 2012, 2013, and 2018 suggest that the partitioning of total N loss
902 must depend on additional yet to be identified environmental or biological interactions.

903

904 **4.5.3 Correlations of percent anammox values to anammox and denitrification rates -** 905 **comparison to previous literature**

906 In order to re-examine the result (Babbin et al., 2020) that enhanced fractions of
907 anammox are correlated to greater anammox rates and not lower denitrification (Fig. 9D right),
908 we created percent anammox vs. anammox and denitrification regressions with the 2018 SR1805
909 and FK180624 data. In 2018, unlike in 2012-13 (Babbin et al., 2020), we observed significant
910 relationships between percent anammox values and both the anammox and denitrification rates
911 (Fig. 9D left). Regressions for the 2012-13 data showed that increases in % anammox values are
912 correlated only to increases in anammox values, not decreases in denitrification (Babbin et al.,
913 2020) (Fig. 9D right). The 2018 regressions, on the other hand, indicate that increases in %
914 anammox are correlated with both increasing anammox and decreasing denitrification rates. The
915 influence of this difference in the 2018 samples can be seen in regressions of % anammox
916 against anammox and denitrification from all three cruises where a similar pattern to the 2018
917 data is observed (Fig. 9C). As above, this indicates a clear difference in the partitioning of
918 anammox and denitrification between the 2018 SR1805 and FK180624 ETNP cruises and the
919 2012-13 TN278 and NBP1305 cruises to the ETNP and ETSP. Despite the significance of the
920 relationships, the low R^2 values indicate that these relationships do not explain most of the

921 variation in the anammox to denitrification ratio. As above, the causal mechanisms behind this
922 variability remains to be elucidated.

923

924 **4.5.4 Caveats about measurements of anammox and denitrification rates**

925 One bias of our sampling scheme for N loss rates is that we do not capture particle
926 adhering denitrifiers. Most denitrifiers that encode the last two steps of denitrification are found
927 on large particles (Ganesh et al., 2013, 2015; Fuchsman et al., 2017). As a result, measurements
928 of complete denitrification from $^{15}\text{NO}_2^-$ to $^{30}\text{N}_2$ that do not capture large particle communities
929 will underestimate the rate. Unfortunately, due to the hydrodynamics of the CTD rosette it is
930 unlikely that large particles will be trapped inside the Niskin bottle. In addition, the nipple of
931 each Niskin is above the bottom of the bottle. As a result, the large particles that are successfully
932 sampled by the CTD sink to the bottom of the Niskin and are not transferred into the experiment
933 (Suter et al., 2017).

934 Another important caveat to some of the above conclusions in section 4.5 is that the
935 detection limits for anammox and denitrification rates are not identical. It is easier to detect
936 anammox for a variety of reasons. For example, anammox from a $^{15}\text{NH}_4^+$ tracer is more easily
937 detected due to low background NH_4^+ across most of the OMZ. Anammox from the $^{15}\text{NO}_2^-$
938 tracer is more detectible due to its reliance on incorporation of only a single ^{15}N atom into the
939 $^{29}\text{N}_2$ product. Denitrification, on the other hand, is more difficult to detect because of higher
940 background NO_2^- concentrations and because definitive denitrification requires the rarer
941 combination of two $^{15}\text{NO}_2^-$ molecules (Babbin et al., 2017).

942 We suspect that our sampling bias against particle based denitrification and
943 denitrification's higher detection limit may have played a role in our observations of

944 denitrification rates in the 2012, 2013, and 2018 cruises where, for example, significant
945 denitrification rates were only detected at four of the thirty depths sampled during SR1805
946 (Supplementary Table S3). As a result, while the comparisons made above are helpful to
947 examine differences in N biogeochemistry across years and stations, the true biogeochemical
948 role of denitrification is likely greater than our tracer experiments suggest.

949 An additional important consideration is the possibility that anammox was stimulated by
950 our tracer additions, which substantially enriched the NO_2^- and especially the NH_4^+
951 concentrations above their in situ values (see Table S7 for enrichment factors for these two
952 nutrients' concentrations). As mentioned above, the differential control of anammox and
953 denitrification by substrate concentration may affect the observed ratio of the two rates in tracer
954 incubations. Tracer additions above ambient nutrient levels are necessary to detect a mass
955 spectrometric signal but often can result in rates above true in situ levels. Data on the kinetic
956 responses of anammox and denitrification are scarce, yet another area where further research
957 would be very useful.

958

959 **4.6 Possibility of N loss via AOA and other N cycling processes**

960 A recent paper (Kraft et al., 2022) reported that dense cultures of the ammonium
961 oxidizing archaea (AOA) *Nitrosopumilus maritimus* can support the O_2 dependent process of
962 NH_4^+ oxidation in deoxygenated waters via NO disproportionation to O_2 and N_2 . This
963 mechanism would be a third N loss process that, if occurring in OMZs, would be measured as
964 anammox or denitrification. In order to investigate the possible significance of this N loss
965 pathway in ODZ waters, we calculated the maximum possible N loss from NH_4^+ oxidation – the
966 N loss that would result if all of the $^{15}\text{N}\text{-NO}_2^-$ produced in our NH_4^+ oxidation experiments was

967 converted into N₂ via the proposed NO disproportionation reaction. These maximum NH₄⁺
968 oxidation derived N loss rates were a small fraction of the total N loss rates at most depths
969 (Supplementary Table S5). As a result, even these unrealistically high estimates of N₂
970 production from AOA do not suggest that AOA are significant agents for fixed N loss. The
971 depths where this was not the case are all either oxic or upper oxycline depths where NH₄⁺
972 oxidation rates peak and do not require NO disproportionation to supply O₂, or depths where
973 equally low NH₄⁺ oxidation, anammox, and denitrification rates would allow a higher percentage
974 of the total N loss to be due to NH₄⁺ oxidation. As a result, our calculation argues that N loss
975 derived from NH₄⁺ oxidation is not a significant N loss flux in ODZs. Thus, we argue that our
976 conclusions regarding the relative balance of anammox and denitrification, as well as the
977 relationship of these two N loss processes to other parts of the N cycle, do not need to be revised
978 to account for N loss via NO disproportionation in AOA.

979 We note that an additional N recycling pathway, dissimilatory nitrate/nitrite reduction to
980 ammonium (DNRA) can occur under low O₂ conditions similar to those preferred by anammox
981 and denitrification. While some OMZ studies have found rates and *nrfA* abundances comparable
982 to anammox, denitrification, and NH₄⁺ oxidation rates and marker gene abundances (Lam et al.,
983 2009; Jensen et al., 2011), DNRA is best described as an extremely variable process. Other past
984 OMZ studies have often found negligible rates (De Brabandere et al., 2014; Kalvelage et al.,
985 2013; Füssel et al., 2011) and little genetic evidence for DNRA (Kalvelage et al., 2013;
986 Fuchsman et al., 2017). Due to this variability we chose to focus this study on what are arguably
987 the most consistently relevant rates for OMZ N biogeochemistry.

988

989 **5 Conclusions**

990 Nitrogen is an essential component of life and as a result, its availability can function as a
991 cap on biological productivity in many marine ecosystems. Since all the ocean is linked through
992 an intricate web of currents that span the globe, the N biogeochemistry of small regions can
993 affect the biogeochemistry of the rest of the ocean. Although OMZs account for just 0.1 - 1% of
994 the ocean's total volume (Lam and Kuypers, 2011; Codispoti and Richards, 1976; Naqvi, 1987;
995 Bange et al., 2000; Codispoti et al., 2005) they account for 30-50% of all total marine N loss
996 (DeVries et al., 2013). As a result, developing an understanding of N cycling within OMZs is
997 critical for comprehending the total marine N budget. Here we presented measurements from the
998 ETNP OMZ of five microbial N cycling metabolisms, all of which have NO_2^- as a product,
999 reactant, or intermediate. Understanding the magnitudes of these rates is key to determining the
1000 OMZ inventory of N species as well as an important piece of understanding the marine N
1001 budget.

1002 Our results add to the growing evidence that the N recycling process of NO_3^- reduction is
1003 the largest OMZ N flux followed by the recycling process of NO_2^- oxidation back to NO_3^- .
1004 These two processes peaked in the oxycline or ODZ top and were usually much greater than the
1005 two N loss processes of anammox and denitrification, a departure from the established view that
1006 understanding N loss processes alone is the key to understanding OMZ biogeochemistry. We
1007 also add further evidence to the body of literature that supports the occurrence of anaerobic NO_2^-
1008 oxidation in OMZ regions, most strikingly through a series of O_2 manipulation experiments that
1009 show NO_2^- oxidation at putative O_2 concentrations as low as 1 nM. We conducted experiments
1010 on waters from two deoxygenated depths to evaluate if NO_2^- dismutation provides the oxidative
1011 power for observed anaerobic NO_2^- oxidation and found no evidence of NO_2^- dismutation except
1012 in one treatment – the closest to in situ NO_2^- conditions. Further exploration of the dismutation

1013 hypothesis might therefore usefully focus on conditions near in situ NO_2^- concentrations. Across
1014 our experiments, the percent of N loss due to anammox was consistently above the theoretical
1015 prediction of at most 29% anammox. Our observations that NO_3^- reduction and NO_2^- oxidation
1016 greatly surpass N loss, especially in shallow boundary waters, further reinforce the view that
1017 NO_2^- in the SNM is sourced from NO_3^- reduction.

1018 Together, these observations provide additional data that supports several new views of
1019 OMZ biogeochemistry. We hope that our work inspires additional isotopic experiments,
1020 culturing efforts, or genomic studies, especially those that seek to further test the occurrence of
1021 NO_2^- oxidation under functionally anoxic conditions and to examine alternative oxidants for this
1022 process. In addition, we emphasize the importance of integrating our experimental results into
1023 future OMZ N and C biogeochemical models, especially our results showing the predominance
1024 of NO_3^- reduction and NO_2^- oxidation over N loss. The development of an accurate model of
1025 OMZ N cycling is essential towards forecasting future changes in marine productivity and
1026 ecology as OMZs respond to climate change and other anthropogenic environmental changes.

1027

1028 **Author contributions**

1029 XS, CF and BBW designed, and CF performed, measured, and calculated the NO_3^- reduction and
1030 NH_4^+ oxidation rates. BBW and JCT designed, BBW and JCT performed, and JCT measured
1031 and calculated the anammox and denitrification depth profile experiments. BBW and XS
1032 designed, JCT, BBW, and XS performed, XS and KD measured, and KD, EW, and JCT
1033 calculated the NO_2^- oxidation depth profiles. TT and ARB designed, TT performed, DEM and
1034 JCT measured, and EW and JCT calculated the anammox and denitrification profiles from the
1035 FK180624 cruise. TT and ARB designed, and TT performed, measured, and calculated the NO_2^-

1036 oxidation O₂ variation experiments. ARB and TT designed, TT performed, EW, XS, and JCT
1037 measured, and EW and JCT calculated the dismutation experiments. SO provided critical help in
1038 running the mass spectrometer to measure all samples except the oxygen variation experiments.
1039 BBW performed the correlation and RDA analyses. JCT drafted the paper with inputs from all
1040 authors.

1041

1042 **Competing Interests**

1043 The authors declare that they have no conflicts of interest.

1044

1045 **Data Availability**

1046 All data discussed in this manuscript is archived at [10.5281/zenodo.7920778](https://doi.org/10.5281/zenodo.7920778).

1047

1048 **Acknowledgments**

1049 We would like to acknowledge the crew and scientists of the R/V *Sally Ride* and the R/V *Falkor*
1050 for logistical and scientific support during our 2018 cruises. We thank Amal Jayakumar for
1051 providing *amoA* and *nirS* gene abundances for the RDA and PCA analyses. We thank Emilio
1052 Robledo-Garcia for assistance using the LUMOS sensor for the NO₂⁻ oxidation O₂ gradient
1053 experiments. We thank Matthias Spieler for supporting NO₃⁻ reduction rate measurements in
1054 Basel. We thank Patrick Boduch for his aid in reviewing graphics before submission. We also
1055 acknowledge the Schmidt Ocean Institute which provided R/V *Falkor* ship time to ARB. We
1056 thank the Simons Foundation and National Science Foundation for supporting ARB, TT, and
1057 DEM on Simons Foundation grant 622065 and NSF grants OCE-2138890 and OCE-2142998 as
1058 well as support for BBW, CF, JCT, and XS through NSF grant OCE-1657663.

1059

1060 **References**

1061 Anderson, J. J., Okubo, A., Robbins, A. S., and Richards, F. A.: A model for nitrate distributions
1062 in oceanic oxygen minimum zones, *Deep Sea Res. Part A. Oceanogr. Res. Pap.*, 29, 1113–1140,
1063 [https://doi.org/10.1016/0198-0149\(82\)90031-0](https://doi.org/10.1016/0198-0149(82)90031-0), 1982.

1064 ASTM International: *Standard Guide for Spiking into Aqueous Samples*, West Conshohocken,
1065 PA, 2006.

1066 Babbin, A. R., Keil, R. G., Devol, A. H., and Ward, B. B.: Organic matter stoichiometry, flux,
1067 and oxygen control nitrogen loss in the ocean, *Science (80-.)*, 344, 406–408,
1068 <https://doi.org/10.1126/science.1248364>, 2014.

1069 Babbin, A. R., Peters, B. D., Mordy, C. W., Widner, B., Casciotti, K. L., and Ward, B. B.:
1070 Multiple metabolisms constrain the anaerobic nitrite budget in the Eastern Tropical South
1071 Pacific, *Global Biogeochem. Cycles*, 31, 258–271, <https://doi.org/10.1002/2016GB005407>,
1072 2017.

1073 Babbin, A. R., Buchwald, C., Morel, F. M. M., Wankel, S. D., and Ward, B. B.: Nitrite oxidation
1074 exceeds reduction and fixed nitrogen loss in anoxic Pacific waters, *Mar. Chem.*, 224, 103814,
1075 <https://doi.org/10.1016/J.MARCHEM.2020.103814>, 2020.

1076 Bange, H. W., Rixen, T., Johansen, A. M., Siefert, R. L., Ramesh, R., Ittekkot, V., Hoffmann, M.
1077 R., and Andreae, M. O.: A revised nitrogen budget of the Arabian Sea, *Global Biogeochem.*
1078 *Cycles*, 14, 1283–1297, <https://doi.org/10.1029/1999GB001228>, 2000.

1079 Beman, J. M., Leilei Shih, J., and Popp, B. N.: Nitrite oxidation in the upper water column and
1080 oxygen minimum zone of the eastern tropical North Pacific Ocean, *ISME J.* 2013 711, 7, 2192–
1081 2205, <https://doi.org/10.1038/ismej.2013.96>, 2013.

1082 Berg, J. S., Ahmerkamp, S., Pjevac, P., Hausmann, B., Milucka, J., and Kuypers, M. M. M.:
1083 How low can they go? Aerobic respiration by microorganisms under apparent anoxia, *FEMS*
1084 *Microbiol. Rev.*, 46, 1–14, <https://doi.org/10.1093/FEMSRE/FUAC006>, 2022.

1085 Bianchi, D., Babbin, A. R., and Galbraith, E. D.: Enhancement of anammox by the excretion of
1086 diel vertical migrators, *Proc. Natl. Acad. Sci.*, 111, 15653–15658,
1087 <https://doi.org/10.1073/PNAS.1410790111>, 2014.

1088 Bock, E., Koops, H. P., Möller, U. C., and Rudert, M.: A new facultatively nitrite oxidizing
1089 bacterium, *Nitrobacter vulgaris* sp. nov., *Arch. Microbiol.* 1990 1532, 153, 105–110,
1090 <https://doi.org/10.1007/BF00247805>, 1990.

1091 De Brabandere, L., Canfield, D. E., Dalsgaard, T., Friederich, G. E., Revsbech, N. P., Ulloa, O.,
1092 and Thamdrup, B.: Vertical partitioning of nitrogen-loss processes across the oxic-anoxic
1093 interface of an oceanic oxygen minimum zone, *Environ. Microbiol.*, 16, 3041–3054,
1094 <https://doi.org/10.1111/1462-2920.12255>, 2014.

1095 Braman, R. S. and Hendrix, S. A.: Nanogram Nitrite and Nitrate Determination in Environmental
1096 and Biological Materials by Vanadium(III) Reduction with Chemiluminescence Detection, *Anal.*
1097 *Chem.*, 61, 2715–2718, 1989.

1098 Brandhorst, W.: Nitrification and Denitrification in the Eastern Tropical North Pacific, *J. du*
1099 *Cons. Cons. Perm. Int. pour l’exploration la mer*, 25, 3–20, 1959.

1100 Bristow, L. A., Dalsgaard, T., Tiano, L., Mills, D. B., Bertagnolli, A. D., Wright, J. J., Hallam, S.
1101 J., Ulloa, O., Canfield, D. E., Revsbech, N. P., and Thamdrup, B.: Ammonium and nitrite
1102 oxidation at nanomolar oxygen concentrations in oxygen minimum zone waters, *Proc. Natl.*
1103 *Acad. Sci. U. S. A.*, 113, 10601–10606, <https://doi.org/10.1073/PNAS.1600359113>, 2016.

1104 Bristow, L. A., Callbeck, C. M., Larsen, M., Altabet, M. A., Dekaezemacker, J., Forth, M.,

1105 Gauns, M., Glud, R. N., Kuypers, M. M. M., Lavik, G., Milucka, J., Naqvi, S. W. A., Pratihary,
1106 A., Revsbech, N. P., Thamdrup, B., Treusch, A. H., and Canfield, D. E.: N₂ production rates
1107 limited by nitrite availability in the Bay of Bengal oxygen minimum zone, *Nat. Geosci.*, 10, 24–
1108 29, <https://doi.org/10.1038/ngeo2847>, 2017.

1109 Buchwald, C. and Wankel, S. D.: Enzyme-catalyzed isotope equilibrium: A hypothesis to
1110 explain apparent N cycling phenomena in low oxygen environments, *Mar. Chem.*, 244, 104140,
1111 <https://doi.org/10.1016/J.MARCHEM.2022.104140>, 2022.

1112 Buchwald, C., Santoro, A. E., Stanley, R. H. R., and Casciotti, K. L.: Nitrogen cycling in the
1113 secondary nitrite maximum of the eastern tropical North Pacific off Costa Rica, *Global*
1114 *Biogeochem. Cycles*, 29, 2061–2081, <https://doi.org/10.1002/2015GB005187>, 2015.

1115 Bulow, S. E., Rich, J. J., Naik, H. S., Pratihary, A. K., and Ward, B. B.: Denitrification exceeds
1116 anammox as a nitrogen loss pathway in the Arabian Sea oxygen minimum zone, *Deep Sea Res.*
1117 *Part I Oceanogr. Res. Pap.*, 57, 384–393, <https://doi.org/10.1016/J.DSR.2009.10.014>, 2010.

1118 Busecke, J. J. M., Resplandy, L., Ditkovsky, S. J., and John, J. G.: Diverging Fates of the Pacific
1119 Ocean Oxygen Minimum Zone and Its Core in a Warming World, *AGU Adv.*, 3,
1120 e2021AV000470, <https://doi.org/10.1029/2021AV000470>, 2022.

1121 Casciotti, K. L.: Inverse kinetic isotope fractionation during bacterial nitrite oxidation, *Geochim.*
1122 *Cosmochim. Acta*, 73, 2061–2076, <https://doi.org/10.1016/J.GCA.2008.12.022>, 2009.

1123 Casciotti, K. L., Buchwald, C., and McIlvin, M.: Implications of nitrate and nitrite isotopic
1124 measurements for the mechanisms of nitrogen cycling in the Peru oxygen deficient zone, *Deep*
1125 *Sea Res. Part I Oceanogr. Res. Pap.*, 80, 78–93, <https://doi.org/10.1016/J.DSR.2013.05.017>,
1126 2013.

1127 Codispoti, L. A. and Packard, T. T.: Denitrification rates in the eastern tropical South Pacific, *J.*

1128 Mar. Res., 38, 453–477, 1980.

1129 Codispoti, L. A. and Richards, F. A.: An analysis of the horizontal regime of denitrification in
1130 the eastern tropical North Pacific, *Limnol. Oceanogr.*, 21, 379–388,
1131 <https://doi.org/10.4319/LO.1976.21.3.0379>, 1976.

1132 Codispoti, L. A., Brandes, J. A., Christensen, J. P., Devol, A. H., Naqvi, S. W. A., Paerl, H. W.,
1133 and Yoshinari, T.: The oceanic fixed nitrogen and nitrous oxide budgets: Moving targets as we
1134 enter the anthropocene?, *Sci. Mar.*, 65, 85–105, <https://doi.org/10.3989/SCIMAR.2001.65S285>,
1135 2001.

1136 Codispoti, L. A., Yoshinari, T., and Devol, A. H.: Suboxic respiration in the oceanic water
1137 column, in: *Respiration in Aquatic Ecosystems*, edited by: del Giorgio, P. A. and Williams, P. J.
1138 L., Oxford University Press, 225–247, 2005.

1139 Cram, J. A., Fuchsman, C. A., Duffy, M. E., Pretty, J. L., Lekanoff, R. M., Neibauer, J. A.,
1140 Leung, S. W., Huebert, K. B., Weber, T. S., Bianchi, D., Evans, N., Devol, A. H., Keil, R. G.,
1141 and McDonnell, A. M. P.: Slow Particle Remineralization, Rather Than Suppressed
1142 Disaggregation, Drives Efficient Flux Transfer Through the Eastern Tropical North Pacific
1143 Oxygen Deficient Zone, *Global Biogeochem. Cycles*, 36, e2021GB007080,
1144 <https://doi.org/10.1029/2021GB007080>, 2022.

1145 Dalsgaard, T., Canfield, D. E., Peterson, J., Thamdrup, B., and Acuna-Gonzales, J.: N production
1146 by anamox in the anoxic water column of Golfo Dulce, Costa Rica., *Nature*, 422, 606–608,
1147 <https://doi.org/10.1038/nature01526>, 2003.

1148 Dalsgaard, T., Thamdrup, B., Farías, L., and Revsbech, N. P.: Anammox and denitrification in
1149 the oxygen minimum zone of the eastern South Pacific, *Limnol. Oceanogr.*, 57, 1331–1346,
1150 <https://doi.org/10.4319/lo.2012.57.5.1331>, 2012.

1151 DeVries, T., Deutsch, C., Rafter, P. A., and Primeau, F.: Marine denitrification rates determined
1152 from a global 3-D inverse model, *Biogeosciences*, 10, 2481–2496, [https://doi.org/10.5194/BG-](https://doi.org/10.5194/BG-10-2481-2013)
1153 10-2481-2013, 2013.

1154 Freitag, A., Rudert, M., and Bock, E.: Growth of *Nitrobacter* by dissimilatoric nitrate reduction,
1155 *FEMS Microbiol. Lett.*, 48, 105–109, <https://doi.org/10.1111/J.1574-6968.1987.TB02524.X>,
1156 1987.

1157 Frey, C., Bange, H. W., Achterberg, E. P., Jayakumar, A., Löscher, C. R., Arévalo-Martínez, D.
1158 L., León-Palmero, E., Sun, M., Sun, X., Xie, R. C., Oleynik, S., and Ward, B. B.: Regulation of
1159 nitrous oxide production in low-oxygen waters off the coast of Peru, *Biogeosciences*, 17, 2263–
1160 2287, <https://doi.org/10.5194/BG-17-2263-2020>, 2020.

1161 Frey, C., Sun, X., Szemberski, L., Casciotti, K. L., Garcia-Robledo, E., Jayakumar, A., Kelly, C.
1162 L., and Lehmann, M. F.: Nitrous oxide production kinetics from ammonia oxidation in the
1163 Eastern Tropical North Pacific, *Limnol. Oceanogr.*, Under review, 2022.

1164 Fuchsman, C. A., Devol, A. H., Saunders, J. K., McKay, C., and Rocap, G.: Niche partitioning of
1165 the N cycling microbial community of an offshore oxygen deficient zone, *Front. Microbiol.*, 8,
1166 2384, <https://doi.org/10.3389/FMICB.2017.02384/BIBTEX>, 2017.

1167 Fuchsman, C. A., Palevsky, H. I., Widner, B., Duffy, M., Carlson, M. C. G., Neibauer, J. A.,
1168 Mulholland, M. R., Keil, R. G., Devol, A. H., and Rocap, G.: Cyanobacteria and cyanophage
1169 contributions to carbon and nitrogen cycling in an oligotrophic oxygen-deficient zone, *ISME J.*
1170 2019 1311, 13, 2714–2726, <https://doi.org/10.1038/s41396-019-0452-6>, 2019.

1171 Füssel, J., Lam, P., Lavik, G., Jensen, M. M., Holtappels, M., Günter, M., and Kuypers, M. M.
1172 M.: Nitrite oxidation in the Namibian oxygen minimum zone, *ISME J.*, 6, 1200–1209,
1173 <https://doi.org/10.1038/ismej.2011.178>, 2011.

1174 Füssel, J., Lücker, S., Yilmaz, P., Nowka, B., van Kessel, M. A. H. J., Bourceau, P., Hach, P. F.,
1175 Littmann, S., Berg, J., Spieck, E., Daims, H., Kuypers, M. M. M., and Lam, P.: Adaptability as
1176 the key to success for the ubiquitous marine nitrite oxidizer *Nitrococcus*, *Sci. Adv.*, 3,
1177 https://doi.org/10.1126/SCIADV.1700807/SUPPL_FILE/1700807_TABLES1_TO_S10.ZIP,
1178 2017.

1179 Ganesh, S., Parris, D. J., Delong, E. F., and Stewart, F. J.: Metagenomic analysis of size-
1180 fractionated picoplankton in a marine oxygen minimum zone, *ISME J.* 2014 81, 8, 187–211,
1181 <https://doi.org/10.1038/ismej.2013.144>, 2013.

1182 Ganesh, S., Bristow, L. A., Larsen, M., Sarode, N., Thamdrup, B., and Stewart, F. J.: Size-
1183 fraction partitioning of community gene transcription and nitrogen metabolism in a marine
1184 oxygen minimum zone, *ISME J.* 2015 912, 9, 2682–2696, <https://doi.org/10.1038/ismej.2015.44>,
1185 2015.

1186 Garcia-Robledo, E., Borisov, S., Klimant, I., and Revsbech, N. P.: Determination of respiration
1187 rates in water with sub-micromolar oxygen concentrations, *Front. Mar. Sci.*, 3, 244,
1188 <https://doi.org/10.3389/FMARS.2016.00244/BIBTEX>, 2016.

1189 Garcia-Robledo, E., Padilla, C. C., Aldunate, M., Stewart, F. J., Ulloa, O., Paulmier, A., Gregori,
1190 G., and Revsbech, N. P.: Cryptic oxygen cycling in anoxic marine zones, *Proc. Natl. Acad. Sci.*
1191 *U. S. A.*, 114, 8319–8324, <https://doi.org/10.1073/PNAS.1619844114>, 2017.

1192 Garcia-Robledo, E., Paulmier, A., Borisov, S. M., and Revsbech, N. P.: Sampling in low oxygen
1193 aquatic environments: The deviation from anoxic conditions, *Limnol. Oceanogr. Methods*, 19,
1194 733–740, <https://doi.org/10.1002/LOM3.10457>, 2021.

1195 Granger, J., & Sigman, D. M.: Removal of nitrite with sulfamic acid for nitrate N and O isotope
1196 analysis with the denitrifier method, *Rapid Commun. Mass Spectrom.*, 23, 3753–3762., *Rapid*

1197 Commun. Mass Spectrom., 23, 3753–3762, <https://doi.org/10.1002/rcm>, 2009.

1198 Granger, J. and Wankel, S. D.: Isotopic overprinting of nitrification on denitrification as a
1199 ubiquitous and unifying feature of environmental nitrogen cycling, Proc. Natl. Acad. Sci. U. S.
1200 A., 113, E6391–E6400,
1201 https://doi.org/10.1073/PNAS.1601383113/SUPPL_FILE/PNAS.201601383SI.PDF, 2016.

1202 Hamersley, M. R., Lavik, G., Woebken, D., Rattray, J. E., Lam, P., Hopmans, E. C., Sinninghe
1203 Damsté, J. S., Krüger, S., Graco, M., Gutiérrez, D., and Kuypers, M. M. M.: Anaerobic
1204 ammonium oxidation in the Peruvian oxygen minimum zone, Limnol. Oceanogr., 52, 923–933,
1205 <https://doi.org/10.4319/LO.2007.52.3.0923>, 2007.

1206 Holmes, R. M., Aminot, A., Kérouel, R., Hooker, B. A., and Peterson, B. J.: A simple and
1207 precise method for measuring ammonium in marine and freshwater ecosystems, Can. J. Fish.
1208 Aquat. Sci., 56, 1801–1808, <https://doi.org/10.1139/f99-128>, 1999.

1209 Horak, R. E. A., Ruef, W., Ward, B. B., and Devol, A. H.: Expansion of denitrification and
1210 anoxia in the eastern tropical North Pacific from 1972 to 2012, Geophys. Res. Lett., 43, 5252–
1211 5260, <https://doi.org/10.1002/2016GL068871>, 2016.

1212 Ito, T., Minobe, S., Long, M. C., and Deutsch, C.: Upper ocean O₂ trends: 1958–2015, Geophys.
1213 Res. Lett., 44, 4214–4223, <https://doi.org/10.1002/2017GL073613>, 2017.

1214 Jayakumar, A., Wajih, S., Naqvi, A., and Ward, B. B.: Distribution and Relative Quantification
1215 of Key Genes Involved in Fixed Nitrogen Loss From the Arabian Sea Oxygen Minimum Zone,
1216 Indian Ocean Biogeochem. Process. Ecol. Var. Geophys. Monogr. Ser., 185,
1217 <https://doi.org/10.1029/2008GM000730>, 2009.

1218 Jensen, M. M., Lam, P., Revsbech, N. P., Nagel, B., Gaye, B., Jetten, M. S. M., and Kuypers, M.
1219 M. M.: Intensive nitrogen loss over the Omani Shelf due to anammox coupled with dissimilatory

1220 nitrite reduction to ammonium, *ISME J.* 2011 510, 5, 1660–1670,
1221 <https://doi.org/10.1038/ismej.2011.44>, 2011.

1222 Kalvelage, T., Lavik, G., Lam, P., Contreras, S., Arteaga, L., Löscher, C. R., Oschlies, A.,
1223 Paulmier, A., Stramma, L., and M Kuypers, M. M.: Nitrogen cycling driven by organic matter
1224 export in the South Pacific oxygen minimum zone, 55812, <https://doi.org/10.1038/NGEO1739>,
1225 2013.

1226 Keeling, R. F., Körtzinger, A., and Gruber, N.: Ocean deoxygenation in a warming world, *Ann.*
1227 *Rev. Mar. Sci.*, 2, 199–229, <https://doi.org/10.1146/annurev.marine.010908.163855>, 2010.

1228 Kemeny, P. C., Weigand, M. A., Zhang, R., Carter, B. R., Karsh, K. L., Fawcett, S. E., and
1229 Sigman, D. M.: Enzyme-level interconversion of nitrate and nitrite in the fall mixed layer of the
1230 Antarctic Ocean, *Global Biogeochem. Cycles*, 30, 1069–1085,
1231 <https://doi.org/10.1002/2015GB005350>, 2016.

1232 Kirstein, K. and Bock, E.: Close genetic relationship between *Nitrobacter hamburgensis* nitrite
1233 oxidoreductase and *Escherichia coli* nitrate reductases, *Arch. Microbiol.* 1993 1606, 160, 447–
1234 453, <https://doi.org/10.1007/BF00245305>, 1993.

1235 Koch, H., Lücker, S., Albertsen, M., Kitzinger, K., Herbold, C., Spieck, E., Nielsen, P. H.,
1236 Wagner, M., and Daims, H.: Expanded metabolic versatility of ubiquitous nitrite-oxidizing
1237 bacteria from the genus *Nitrospira*, *Proc. Natl. Acad. Sci. U. S. A.*, 112, 11371–11376,
1238 <https://doi.org/10.1073/PNAS.1506533112>, 2015.

1239 Kondo, Y. and Moffett, J. W.: Iron redox cycling and subsurface offshore transport in the eastern
1240 tropical South Pacific oxygen minimum zone, *Mar. Chem.*, 168, 95–103,
1241 <https://doi.org/10.1016/J.MARCHEM.2014.11.007>, 2015.

1242 Kraft, B., Jehmlich, N., Larsen, M., Bristow, L. A., Könneke, M., Thamdrup, B., and Canfield,

1243 D. E.: Oxygen and nitrogen production by an ammonia-oxidizing archaeon, *Science* (80-.), 375,
1244 97–100,
1245 https://doi.org/10.1126/SCIENCE.ABE6733/SUPPL_FILE/SCIENCE.ABE6733_MDAR_REPR
1246 [ODUCIBILITY_CHECKLIST.PDF](https://doi.org/10.1126/SCIENCE.ABE6733/SUPPL_FILE/SCIENCE.ABE6733_MDAR_REPR), 2022.

1247 Kuenen, J. G.: Anammox bacteria from discovery, 6, <https://doi.org/10.1038/nrmicro1857>, 2008.

1248 Kuypers, M. M. M., Lavik, G., Woebken, D., Schmid, M., Fuchs, B. M., Amann, R., Jørgensen,
1249 B. B., and Jetten, M. S. M.: Massive nitrogen loss from the Benguela upwelling system through
1250 anaerobic ammonium oxidation, *Proc. Natl. Acad. Sci. U. S. A.*, 102, 6478–6483,
1251 <https://doi.org/10.1073/PNAS.0502088102>, 2005.

1252 Lam, P. and Kuypers, M. M. M.: Microbial Nitrogen Cycling Processes in Oxygen Minimum
1253 Zones, *Ann. Rev. Mar. Sci.*, 3, 317–345, <https://doi.org/10.1146/annurev-marine-120709->
1254 [142814](https://doi.org/10.1146/annurev-marine-120709-), 2011.

1255 Lam, P., Lavik, G., Jensen, M. M., Van Vossenberg, J. De, Schmid, M., Woebken, D., Gutiérrez,
1256 D., Amann, R., Jetten, M. S. M., and Kuypers, M. M. M.: Revising the nitrogen cycle in the
1257 Peruvian oxygen minimum zone, *Proc. Natl. Acad. Sci. U. S. A.*, 106, 4752–4757,
1258 <https://doi.org/10.1073/PNAS.0812444106>, 2009.

1259 Lam, P., Jensen, M. M., Kock, A., Lettmann, K. A., Plancherel, Y., Lavik, G., Bange, H. W., and
1260 Kuypers, M. M. M.: Origin and fate of the secondary nitrite maximum in the Arabian Sea,
1261 *Biogeosciences*, 8, 1565–1577, <https://doi.org/10.5194/BG-8-1565-2011>, 2011.

1262 Van de Leemput, I. A., Veraart, A. J., Dakos, V., De Klein, J. J. M., Strous, M., and Scheffer,
1263 M.: Predicting microbial nitrogen pathways from basic principles, *Environ. Microbiol.*, 13,
1264 1477–1487, <https://doi.org/10.1111/J.1462-2920.2011.02450.X>, 2011.

1265 Lehner, P., Larndorfer, C., Garcia-Robledo, E., Larsen, M., Borisov, S. M., Revsbech, N. P.,

1266 Glud, R. N., Canfield, D. E., and Klimant, I.: LUMOS - A Sensitive and Reliable Optode System
1267 for Measuring Dissolved Oxygen in the Nanomolar Range, *PLoS One*, 10, e0128125,
1268 <https://doi.org/10.1371/JOURNAL.PONE.0128125>, 2015.

1269 Lipschultz, F., Wofsy, S. C., Ward, B. B., Codispoti, L. A., Friedrich, G., and Elkins, J. W.:
1270 Bacterial transformations of inorganic nitrogen in the oxygen-deficient waters of the Eastern
1271 Tropical South Pacific Ocean, *Deep Sea Res. Part A. Oceanogr. Res. Pap.*, 37, 1513–1541,
1272 [https://doi.org/10.1016/0198-0149\(90\)90060-9](https://doi.org/10.1016/0198-0149(90)90060-9), 1990.

1273 Lomas, M. W. and Lipschultz, F.: Forming the primary nitrite maximum: Nitrifiers or
1274 phytoplankton?, *Limnol. Oceanogr.*, 51, 2453–2467, <https://doi.org/10.4319/LO.2006.51.5.2453>,
1275 2006.

1276 Luther, G. W.: The role of one- and two-electron transfer reactions in forming
1277 thermodynamically unstable intermediates as barriers in multi-electron redox reactions, *Aquat.*
1278 *Geochemistry*, 16, 395–420, <https://doi.org/10.1007/S10498-009-9082-3/FIGURES/14>, 2010.

1279 Luther, G. W. and Popp, J. I.: Kinetics of the Abiotic Reduction of Polymeric Manganese
1280 Dioxide by Nitrite: An Anaerobic Nitrification Reaction, *Aquat. Geochemistry* 2002 81, 8, 15–
1281 36, <https://doi.org/10.1023/A:1020325604920>, 2002.

1282 Margolskee, A., Frenzel, H., Emerson, S., and Deutsch, C.: Ventilation Pathways for the North
1283 Pacific Oxygen Deficient Zone, *Global Biogeochem. Cycles*, 33, 875–890,
1284 <https://doi.org/10.1029/2018GB006149>, 2019.

1285 Martin, J. H., Knauer, G. A., Karl, D. M., and Broenkow, W. W.: VERTEX: carbon cycling in
1286 the northeast Pacific, *Deep Sea Res. Part A. Oceanogr. Res. Pap.*, 34, 267–285,
1287 [https://doi.org/10.1016/0198-0149\(87\)90086-0](https://doi.org/10.1016/0198-0149(87)90086-0), 1987.

1288 McIlvin, M. R. and Altabet, M. A.: Chemical conversion of nitrate and nitrite to nitrous oxide for

1289 nitrogen and oxygen isotopic analysis in freshwater and seawater, *Anal. Chem.*, 77, 5589–5595,
1290 <https://doi.org/10.1021/ac050528s>, 2005.

1291 Mincer, T. J., Church, M. J., Taylor, L. T., Preston, C., Karl, D. M., and DeLong, E. F.:
1292 Quantitative distribution of presumptive archaeal and bacterial nitrifiers in Monterey Bay and the
1293 North Pacific Subtropical Gyre, *Environ. Microbiol.*, 9, 1162–1175,
1294 <https://doi.org/10.1111/J.1462-2920.2007.01239.X>, 2007.

1295 Moriyasu, R., Evans, N., Bolster, K. M., Hardisty, D. S., and Moffett, J. W.: The Distribution
1296 and Redox Speciation of Iodine in the Eastern Tropical North Pacific Ocean, *Global
1297 Biogeochem. Cycles*, 34, e2019GB006302, <https://doi.org/10.1029/2019GB006302>, 2020.

1298 Naqvi, S. W. A.: Some aspects of the oxygen-deficient conditions and denitrification in the
1299 Arabian Sea, *J. Mar. Res.*, 45, 1049–1072, 1987.

1300 Nozaki, Y.: A fresh look at element distribution in the North Pacific Ocean, *Eos, Trans. Am.
1301 Geophys. Union*, 78, 221–221, <https://doi.org/10.1029/97EO00148>, 1997.

1302 Oshiki, M., Satoh, H., and Okabe, S.: Ecology and physiology of anaerobic ammonium oxidizing
1303 bacteria, *Environ. Microbiol.*, 18, 2784–2796, [https://doi.org/10.1111/1462-
1304 2920.13134/SUPPINFO](https://doi.org/10.1111/1462-2920.13134/SUPPINFO), 2016.

1305 Padilla, C. C., Bristow, L. A., Sarode, N., Garcia-Robledo, E., Gómez Ramírez, E., Benson, C.
1306 R., Bourbonnais, A., Altabet, M. A., Girguis, P. R., Thamdrup, B., and Stewart, F. J.: NC10
1307 bacteria in marine oxygen minimum zones, *ISME J.* 2016 108, 10, 2067–2071,
1308 <https://doi.org/10.1038/ismej.2015.262>, 2016.

1309 Peng, X., Fuchsman, C. A., Jayakumar, A., Oleynik, S., Martens-Habbena, W., Devol, A. H., and
1310 Ward, B. B.: Ammonia and nitrite oxidation in the Eastern Tropical North Pacific, *Global
1311 Biogeochem. Cycles*, 29, 2034–2049, <https://doi.org/10.1002/2015GB005278>, 2015.

1312 Peng, X., Fuchsman, C. A., Jayakumar, A., Warner, M. J., Devol, A. H., and Ward, B. B.:
1313 Revisiting nitrification in the Eastern Tropical South Pacific: A focus on controls, *J. Geophys.*
1314 *Res. Ocean.*, 121, 1667–1684, <https://doi.org/10.1002/2015JC011455>, 2016.

1315 Penn, J., Weber, T., and Deutsch, C.: Microbial functional diversity alters the structure and
1316 sensitivity of oxygen deficient zones, *Geophys. Res. Lett.*, 43, 9773–9780,
1317 <https://doi.org/10.1002/2016GL070438>, 2016.

1318 Peters, B. D., Babbin, A. R., Lettmann, K. A., Mordy, C. W., Ulloa, O., Ward, B. B., and
1319 Casciotti, K. L.: Vertical modeling of the nitrogen cycle in the eastern tropical South Pacific
1320 oxygen deficient zone using high-resolution concentration and isotope measurements, *Global*
1321 *Biogeochem. Cycles*, 30, 1661–1681, <https://doi.org/10.1002/2016GB005415>, 2016.

1322 R: A language and environment for statistical computing:
1323 Starkenburg, S. R., Larimer, F. W., Stein, L. Y., Klotz, M. G., Chain, P. S. G., Sayavedra-Soto,
1324 L. A., Poret-Peterson, A. T., Gentry, M. E., Arp, D. J., Ward, B., and Bottomley, P. J.: Complete
1325 genome sequence of *Nitrobacter hamburgensis* X14 and comparative genomic analysis of
1326 species within the genus *Nitrobacter*, *Appl. Environ. Microbiol.*, 74, 2852–2863,
1327 https://doi.org/10.1128/AEM.02311-07/SUPPL_FILE/SUPPLEMENTAL_TABLE_2.PDF,
1328 2008.

1329 Stramma, L., Johnson, G. C., Sprintall, J., and Mohrholz, V.: Expanding oxygen-minimum zones
1330 in the tropical oceans, *Science (80-.)*, 320, 655–658,
1331 [https://doi.org/10.1126/SCIENCE.1153847/ASSET/09F7EF41-9228-40BD-8E17-
1332 06C4E9218CC5/ASSETS/GRAPHIC/320_655_F2.JPEG](https://doi.org/10.1126/SCIENCE.1153847/ASSET/09F7EF41-9228-40BD-8E17-06C4E9218CC5/ASSETS/GRAPHIC/320_655_F2.JPEG), 2008.

1333 Strickland, J. D. H. and Parsons, T. R.: *A Practical Handbook of Seawater Analysis*, Fisheries
1334 Research Board of Canada, Ottawa, 1972.

1335 Strohm, T. O., Griffin, B., Zumft, W. G., and Schink, B.: Growth yields in bacterial
1336 denitrification and nitrate ammonification, *Appl. Environ. Microbiol.*, 73, 1420–1424,
1337 [https://doi.org/10.1128/AEM.02508-06/ASSET/88AA1997-7BB3-42B6-A761-](https://doi.org/10.1128/AEM.02508-06/ASSET/88AA1997-7BB3-42B6-A761-DCB47D972CA6/ASSETS/GRAPHIC/ZAM0050775730001.JPEG)
1338 [DCB47D972CA6/ASSETS/GRAPHIC/ZAM0050775730001.JPEG](https://doi.org/10.1128/AEM.02508-06/ASSET/88AA1997-7BB3-42B6-A761-DCB47D972CA6/ASSETS/GRAPHIC/ZAM0050775730001.JPEG), 2007.

1339 Strous, M., Heijnen, J. J., Kuenen, J. G., and Jetten, M. S. M.: The sequencing batch reactor as a
1340 powerful tool for the study of slowly growing anaerobic ammonium-oxidizing microorganisms,
1341 *Appl. Microbiol. Biotechnol.* 1998 505, 50, 589–596, <https://doi.org/10.1007/S002530051340>,
1342 1998.

1343 Sun, X. and Ward, B. B.: Novel metagenome-assembled genomes involved in the nitrogen cycle
1344 from a Pacific oxygen minimum zone, *ISME Commun.* 2021 11, 1, 1–5,
1345 <https://doi.org/10.1038/s43705-021-00030-2>, 2021.

1346 Sun, X., Ji, Q., Jayakumar, A., and Ward, B. B.: Dependence of nitrite oxidation on nitrite and
1347 oxygen in low-oxygen seawater, *Geophys. Res. Lett.*, 44, 7883–7891,
1348 <https://doi.org/10.1002/2017GL074355>, 2017.

1349 Sun, X., Kop, L. F. M., Lau, M. C. Y., Frank, J., Jayakumar, A., Lückner, S., and Ward, B. B.:
1350 Uncultured Nitrospina-like species are major nitrite oxidizing bacteria in oxygen minimum
1351 zones, *ISME J.*, <https://doi.org/10.1038/s41396-019-0443-7>, 2019.

1352 Sun, X., Frey, C., Garcia-Robledo, E., Jayakumar, A., and Ward, B. B.: Microbial niche
1353 differentiation explains nitrite oxidation in marine oxygen minimum zones, *ISME J.* 2021 155,
1354 15, 1317–1329, <https://doi.org/10.1038/s41396-020-00852-3>, 2021.

1355 Sun, X., Frey, C., and Ward, B. B.: Nitrite Oxidation Across the Full Oxygen Spectrum in the
1356 Ocean, *Global Biogeochem. Cycles*, 37, e2022GB007548,
1357 <https://doi.org/10.1029/2022GB007548>, 2023.

1358 Suter, E. A., Scranton, M. I., Chow, S., Stinton, D., Medina Faull, L., and Taylor, G. T.: Niskin
1359 bottle sample collection aliases microbial community composition and biogeochemical
1360 interpretation, *Limnol. Oceanogr.*, 62, 606–617, <https://doi.org/10.1002/LNO.10447>, 2017.

1361 Tang, W., Tracey, J. C., Carroll, J., Wallace, E., Lee, J. A., Nathan, L., Sun, X., Jayakumar, A.,
1362 and Ward, B. B.: Nitrous oxide production in the Chesapeake Bay, *Limnol. Oceanogr.*, 67,
1363 2101–2116, <https://doi.org/10.1002/LNO.12191>, 2022.

1364 Taylor, B. W., Keep, C. F., Hall, R. O., Koch, B. J., Tronstad, L. M., Flecker, A. S., and Ulseth,
1365 A. J.: Improving the fluorometric ammonium method: matrix effects, background fluorescence,
1366 and standard additions, *Am. Benthol. Soc.*, 26, 167–177, <https://doi.org/10.1899/0887-3593>,
1367 2007.

1368 Thamdrup, B. and Dalsgaard, T.: The fate of ammonium in anoxic manganese oxide-rich marine
1369 sediment, *Geochim. Cosmochim. Acta*, 64, 4157–4164, <https://doi.org/10.1016/S0016->
1370 [7037\(00\)00496-8](https://doi.org/10.1016/S0016-7037(00)00496-8), 2000.

1371 Thamdrup, B. and Dalsgaard, T.: Production of N₂ through anaerobic ammonium oxidation
1372 coupled to nitrate reduction in marine sediments, *Appl. Environ. Microbiol.*, 68, 1312–1318,
1373 <https://doi.org/10.1128/AEM.68.3.1312-1318.2002/ASSET/F1579424-64C0-464C-AF9C->
1374 [5BEB3458C869/ASSETS/GRAPHIC/AM0321630005.JPEG](https://doi.org/10.1128/AEM.68.3.1312-1318.2002/ASSET/F1579424-64C0-464C-AF9C-5BEB3458C869/ASSETS/GRAPHIC/AM0321630005.JPEG), 2002.

1375 Thamdrup, B., Dalsgaard, T., Jensen, M. M., Ulloa, O., Farías, L., and Escribano, R.: Anaerobic
1376 ammonium oxidation in the oxygen-deficient waters off northern Chile, *Limnol. Oceanogr.*, 51,
1377 2145–2156, <https://doi.org/10.4319/LO.2006.51.5.2145>, 2006.

1378 Tiano, L., Garcia-Robledo, E., Dalsgaard, T., Devol, A. H., Ward, B. B., Ulloa, O., Canfield, D.
1379 E., and Peter Revsbech, N.: Oxygen distribution and aerobic respiration in the north and south
1380 eastern tropical Pacific oxygen minimum zones, *Deep Sea Res. Part I Oceanogr. Res. Pap.*, 94,

1381 173–183, <https://doi.org/10.1016/J.DSR.2014.10.001>, 2014.

1382 Tsementzi, D., Wu, J., Deutsch, S., Nath, S., Rodriguez-R, L. M., Burns, A. S., Ranjan, P.,
1383 Sarode, N., Malmstrom, R. R., Padilla, C. C., Stone, B. K., Bristow, L. A., Larsen, M., Glass, J.
1384 B., Thamdrup, B., Woyke, T., Konstantinidis, K. T., and Stewart, F. J.: SAR11 bacteria linked to
1385 ocean anoxia and nitrogen loss, *Nature*, 536, 179–183, <https://doi.org/10.1038/nature19068>,
1386 2016.

1387 Ulloa, O., Canfield, D. E., DeLong, E. F., Letelier, R. M., and Stewart, F. J.: Microbial
1388 oceanography of anoxic oxygen minimum zones, *Proc. Natl. Acad. Sci. U. S. A.*, 109, 15996–
1389 16003, <https://doi.org/10.1073/PNAS.1205009109>, 2012.

1390 Vedamati, J., Chan, C., and Moffett, J. W.: Distribution of dissolved manganese in the Peruvian
1391 Upwelling and Oxygen Minimum Zone, *Geochim. Cosmochim. Acta*, 156, 222–240,
1392 <https://doi.org/10.1016/J.GCA.2014.10.026>, 2015.

1393 Wanninkhof, R.: Relationship between wind speed and gas exchange over the ocean, *J. Geophys.*
1394 *Res. Ocean.*, 97, 7373–7382, <https://doi.org/10.1029/92JC00188>, 1992.

1395 Ward, B. B., Glover, H. E., and Lipschultz, F.: Chemoautotrophic activity and nitrification in the
1396 oxygen minimum zone off Peru, *Deep Sea Res. Part A. Oceanogr. Res. Pap.*, 36, 1031–1051,
1397 [https://doi.org/10.1016/0198-0149\(89\)90076-9](https://doi.org/10.1016/0198-0149(89)90076-9), 1989.

1398 Ward, B. B., Tuit, C. B., Jayakumar, A., Rich, J. J., Moffett, J., and Naqvi, S. W. A.: Organic
1399 carbon, and not copper, controls denitrification in oxygen minimum zones of the ocean, *Deep*
1400 *Sea Res. Part I Oceanogr. Res. Pap.*, 55, 1672–1683, <https://doi.org/10.1016/J.DSR.2008.07.005>,
1401 2008.

1402 Ward, B. B., Devol, A. H., Rich, J. J., Chang, B. X., Bulow, S. E., Naik, H., Pratihary, A., and
1403 Jayakumar, A.: Denitrification as the dominant nitrogen loss process in the Arabian Sea, *Nat.*

1404 2009 4617260, 461, 78–81, <https://doi.org/10.1038/nature08276>, 2009.

1405 Weigand, M. A., Foriel, J., Barnett, B., Oleynik, S., and Sigman, D. M.: Updates to
1406 instrumentation and protocols for isotopic analysis of nitrate by the denitrifier method, *Rapid*
1407 *Commun. Mass Spectrom.*, 30, 1365–1383, <https://doi.org/10.1002/rcm.7570>, 2016.

1408 Wunderlich, A., Meckenstock, R. U., and Einsiedl, F.: A mixture of nitrite-oxidizing and
1409 denitrifying microorganisms affects the $\delta^{18}\text{O}$ of dissolved nitrate during anaerobic microbial
1410 denitrification depending on the $\delta^{18}\text{O}$ of ambient water, *Geochim. Cosmochim. Acta*, 119, 31–
1411 45, <https://doi.org/10.1016/J.GCA.2013.05.028>, 2013.

1412